Youth-associated protein TIMP2 alters microglial state and function in the context of aging

Brittany M. Hemmer[1,2,3,4,5], Ana Catarina Ferreira[1,2,3,4], Sarah M. Philippi[1,2,3,4,5], Samuele F. Petridis[1,2,3,4], Annie Phan[1,2,3,4], Joseph M. Castellano[1,2,3,4]*

[1]Nash Family Department of Neuroscience, Friedman Brain Institute, Icahn School of Medicine at Mount Sinai, New York, NY, USA

[2]Ronald M. Loeb Center for Alzheimer's Disease, Icahn School of Medicine at Mount Sinai, New York, NY, USA

[3]Department of Neurology, Icahn School of Medicine at Mount Sinai, New York, NY, USA

[4]Black Family Stem Cell Institute, Icahn School of Medicine at Mount Sinai, New York, NY, USA

[5]Graduate School of Biomedical Sciences, Icahn School of Medicine at Mount Sinai, New York, NY, USA

*Correspondence:

Joseph Castellano, Ph.D.

Icahn School of Medicine at Mount Sinai

1425 Madison Avenue, Box 1065

Phone: 212-659-5913

E-mail: joseph.castellano@mssm.edu

Abstract

There is little understanding of how aging serves as the strongest risk factor for Alzheimer's disease (AD) and other neurological disorders. Specific neural cell types, such as microglia, undergo maladaptive changes with age, including increased inflammation, impaired debris clearance, and cellular senescence, yet specific mediators that regulate these processes remain unclear. The aged brain is rejuvenated by youth-associated plasma factors, including tissue inhibitor of metalloproteinases 2 (TIMP2), which we have shown acts on the extracellular matrix (ECM) to regulate synaptic plasticity. Given emerging roles for microglia in regulating plasticity and brain ECM dynamics, we examined the impact of TIMP2 on microglial function in the setting of aging. We show that TIMP2 deletion exacerbates microglial phenotypes associated with aging, including transcriptomic changes in cell activation, increased microgliosis, and increased levels of stress and inflammatory proteins measured in the brain extracellular space by *in vivo* microdialysis. Deleting specific cellular pools of TIMP2 *in* vivo increased microglial activation and altered myelin phagocytosis. Treating aged mice with TIMP2 reversed several phenotypes observed in our deletion models, resulting in decreased microglial activation, reduced proportions of proinflammatory microglia, and enhanced synapse phagocytosis. Our results identify TIMP2 as a key modulator of age-associated microglia dysfunction. Harnessing its activity may mitigate detrimental effects of age-associated insults on microglia function.

Introduction

Aging is accompanied by progressive functional decline across multiple organ systems, but its impact on the brain is especially devastating given the dysfunction wrought across key cognitive domains and the increased risk it poses for several neurological disorders. These changes reflect cumulative cellular, molecular, and structural perturbations, including decreased generation of newborn neurons, loss of synaptic and myelin integrity, and microgliosis in vulnerable brain regions like the hippocampus. Understanding mechanisms that regulate aging in the

49 hippocampus is thus essential for identifying new strategies to preserve or restore function across
50 lifespan and to limit risk for neurological disease. Interestingly, the process of aging and AD pose
51 similar challenges to the brain's immune environment, including aberrant inflammation and
52 elevated exposure to lipid-rich debris from dying cells[1]. The role of microglia, the brain's innate
53 immune cells, in responding to aging-associated damage has emerged as a promising avenue
54 for investigation, galvanized by the identification of many myeloid-enriched genes associated with
55 AD risk in a series of GWAS over the past decade[2]. While specific states adopted by microglia
56 may initially be protective to limit pathology to surrounding brain tissue, chronic challenges and
57 exposure to debris may create maladaptive responses,[3-6] which manifests as phagocytic
58 ineptitude[7-10], production of inflammatory cytokines[11,12], and increased stress responses[6,13]. Thus,
59 there is a need to identify means to rejuvenate the response of these cells to aging-associated
60 challenges to provide a path for novel therapies that limit the impact of aging on neurological
61 disorders.
62
63 Modulating the systemic environment has emerged as a promising strategy to counteract age-
64 related decline in cellular function. Exposure to factors present within young blood rejuvenates
65 the aged brain[14,15], leading to increased synaptic plasticity[16-18] and dendritic spine integrity[17],
66 enhanced vascular remodeling[19], and improved learning and memory performance in aged
67 mice[16-18]. While much of this work has focused on the impact of blood-borne factors directly on
68 neurons or adult neuroblasts in the hippocampus, recent work has suggested that microglia can
69 take up labeled proteins originating in plasma[20,21], suggesting that they may be responsive to
70 blood-borne factors. Moreover, in response to treatment with plasma or a platelet factor that acts
71 on immune cells in the periphery, microglia appear to exhibit altered phagocytosis[21] and activation
72 state[18], respectively. Despite these intriguing findings, the field lacks detailed characterization of
73 how specific youth-associated factors affect microglial function and how such factors can be
74 harnessed to revitalize the aged brain.

75

76 We previously identified tissue inhibitor of metalloproteinases 2 (TIMP2) as a youth-associated
77 blood-borne factor that is capable of revitalizing hippocampal function in aged mice[16]. Levels of
78 TIMP2 are elevated in very young human and mouse plasma and rapidly decline into adulthood
79 and old age[16]. Interestingly, a recent study finds that those expressing *TIMP2* variants associated
80 with higher plasma levels exhibit higher cognitive performance in a cohort of aged individuals[22].
81 Aged mice treated systemically with TIMP2 exhibit similar improvements as mice treated with
82 young plasma, including increased hippocampal plasticity and cognitive improvements, likely as
83 a result of direct TIMP2 action on CNS cells given its entry from blood into brain[16]. While TIMP2
84 has many canonical and non-canonical targets[23,24], these studies suggest that TIMP2 has myriad
85 roles within the hippocampal microenvironment, and its role in modulating innate immune function
86 is understudied. We recently reported that TIMP2 plays a critical role in the young hippocampus
87 in regulating memory, synaptic integrity, and adult neurogenesis through modulation of ECM
88 homeostasis[25], processes that have been found to be regulated by microglia[26,27]. Given the
89 modulation by TIMP2 in processes linked to microglia function and the rejuvenating capacity of
90 TIMP2 in aging contexts, we sought to determine how TIMP2 affects basic microglial function and
91 whether systemic supplementation can restore protective microglial activities that are lost with
92 exposure to age-associated insults.

93

94 Here we show that loss of TIMP2 expression from a variety of sources (i.e., removal from global,
95 microglial, and neuronal sources) alters microglia by increasing activation, elevating their
96 inflammatory state, and shifting phagocytosis—all processes associated with aging. Restoring the
97 extrinsic pool of TIMP2 in aged mice through systemic TIMP2 treatment reversed these age-
98 associated phenotypes by reducing microgliosis and specific inflammatory microglial
99 subpopulations and by enhancing synapse phagocytosis in the hippocampus. Together our
100 results demonstrate that the youth-associated protein TIMP2 plays a novel role in modulating

101 microglial function by shifting their responses to accommodate detrimental aging pathologies in a
102 protective fashion. This work firmly positions TIMP2 as a relevant therapeutic target to limit aging
103 pathology and highlights the need for further mechanistic investigation into how systemic factors
104 modulate innate immune function in the brain.
105
106 **Results**
107
108 **Early deletion of TIMP2 alters microglial state**
109 TIMP2 is expressed in cells of the periphery, contributing to high levels in the plasma[16], and also
110 hippocampal neurons within the CNS[25], with expression in both compartments declining with
111 age[16]. Interestingly, *Timp2* has been shown to be upregulated in subpopulations of microglia in
112 response to aging and AD pathology as part of a panel of genes termed the disease-associated
113 microglia (DAM) profile[28]. To explore its expression within microglia, we noted its enriched
114 transcript abundance within microglia in published transcriptomic atlases, including in *Tabula*
115 *Muris Senis*[29], and in the Allen Brain Cell scRNAseq and MERFISH Atlas[30], in which *Timp2* is
116 expressed at high levels in the brain, particularly in hippocampal microglia (**Supplementary Fig.**
117 **1a-c**). To begin to characterize whether microglia express TIMP2 at the protein level and how its
118 loss influences function at early stages, we isolated primary microglia from neonatal forebrain
119 from wild-type (WT) and TIMP2 knock-out (KO) mice (**Fig. 1a**) at an age when global TIMP2 levels
120 are high[16]. We find high levels of TIMP2 protein by both immunoblotting of primary microglia
121 lysates and immunocytochemistry (ICC), whereas TIMP2 was not detected in TIMP2 KO microglia
122 (**Fig. 1b-c**). We next sought to understand what pathways may be disrupted by its loss in microglia
123 by performing bulk RNA-sequencing on WT and KO primary microglia (**Fig. 1a**). As expected, KO
124 microglia lacked *Timp2* transcript, (**Fig. 1d**) and we detected a number of differentially expressed
125 genes in KO microglia relative to WT (252 upregulated, 316 downregulated; **Supplementary Fig.**
126 **1d**). To gain insight into what pathways are perturbed in microglia by TIMP2 deletion, we

127 performed over-representation analyses for gene ontology (GO)[31] terms related to 'biological
128 processes' and 'cellular components'. Genes that were upregulated in KO microglia were
129 significantly enriched in terms for "cell activation involved in immune response" and "positive
130 regulation of cytokine production", among others (**Fig. 1e**). Downregulated DEGs in KO microglia
131 were significantly enriched in pathways related to "synapse" and "neurogenesis" (**Fig. 1e**). The
132 transcriptomic profile of KO microglia may reflect a more activated and perhaps inflammatory
133 state relative to WT microglia, potentially regulating their communication with neurons and ability
134 to promote plasticity, as suggested in perturbed pathways identified by Ingenuity Pathway
135 Analysis (IPA) (**Supplementary Fig. 1e)**.

136 Given TIMP2's potential relationship with activation state, we stained cultures of primary
137 microglia isolated from adult mice and found that the majority of TIMP2-expressing cells co-
138 express CD68, a lysosomal-associated protein found enriched in myeloid cells (**Fig. 1f-g),**
139 pointing to a potential role for TIMP2 in regulating lysosomal function or activation state. While
140 not all microglia were found to express TIMP2, a sizeable fraction of microglia expressing CD68
141 co-expressed TIMP2 (**Supplementary Fig. 1f-h**).

142

143 **TIMP2 deletion increases hippocampal microgliosis and extracellular inflammatory**
144 **proteins**

145 To evaluate the extent to which the putative pathways identified in our profiling of KO and WT
146 microglia may reflect microglial phenotypes *in vivo* consistent with elevated activation state, we
147 next sought to characterize microglial activation in KO and WT dentate gyrus of the adult
148 hippocampus, a relevant region based on previous work demonstrating its role in regulating
149 plasticity processes[16,25]. Using confocal microscopy, we evaluated microglia by co-staining for
150 microglia marker IBA1 and activation marker CD68, which we previously found co-expressed with
151 TIMP2 in primary microglia (**Fig. 1f-g**). As early as 3-4 months of age, KO mice exhibited a trend
152 towards an increase in the percentage of dentate gyrus (DG) covered by IBA1 staining relative to

153 WT (**Fig. 2a-b**), perhaps reflecting early changes in microglial morphology. While levels were
154 modestly low given the early age, we detected significantly more microglia co-expressing CD68
155 in KO dentate gyrus compared to that from WT mice (**Fig. 2a,c**), as well as higher percentage
156 area covered by CD68 (**Supplementary Fig. 2a-b)**, indicating increased microgliosis. TIMP2
157 deletion did not affect the total number of microglia (**Supplementary Fig. 2a,c)**.

158 We next examined if these changes persist or worsen at a later age, given the well-
159 established age-dependent microgliosis that occurs in the hippocampus[32]. At 6-7 months of age,
160 we found that while the total number of microglia was not affected by TIMP2 deletion
161 (**Supplementary Fig. 2d-e)**, the percentage of DG area occupied by IBA1 immunoreactivity was
162 significantly higher in the DG of TIMP2 KO compared to WT DG (**Fig. 2d-e**). To further
163 characterize this change, we performed a morphology analysis that broadly categorizes microglia
164 as "ramified", "activated", or "ameboid" based on their circularity using an established method
165 (**Supplementary Fig. 2f**)[33-36]. Our morphology analysis revealed an increased number of
166 morphologically "activated" microglia in the DG of KO mice relative to WT, with no change in the
167 number of "ramified" or "ameboid" microglia (**Supplementary Fig. 2g-j**). At this age, we also
168 detected a robust elevation in the number of $IBA1^{+}CD68^{+}$ cells in the DG of KO mice compared
169 to WT, reflecting the increased state of activation (**Fig. 2d,f**).

170 In inflammatory contexts, it is well-established that microglia release cytokines and other
171 factors into the extracellular space, affecting the cellular microenvironment of the brain. Given the
172 increased microgliosis found in KO hippocampus, we next sought to assess whether deletion of
173 TIMP2 alters the extracellular milieu. Conventional tissue-based assessment of cytokines and
174 chemokines do not accurately reflect the composition of the brain interstitial fluid (ISF) given loss
175 of compartmental barriers and effects of extraction methods on sensitivity, and this approach is
176 limited to postmortem sampling, which may not sufficiently capture the dynamics of immune
177 changes. To circumvent these issues, we employed high molecular-weight cut-off (HMWCO; 1-
178 MDa) *in vivo* microdialysis to sample the hippocampal ISF of awake and freely moving mice (**Fig.**

179 **2g**)[37,38]. This technique has not yet been rigorously applied to measure brain immune proteins,
180 which are typically present in the brain ISF at very low levels. To establish this method's potential
181 to examine immune-related proteins in the brain ISF, we administered a single systemic injection
182 of lipopolysaccardine (LPS; 5 mg/kg), an established pro-inflammatory stimulus[39], as a proof-of-
183 concept approach in a 5XFAD model of amyloid pathology that should exhibit high baseline
184 cytokine and chemokine levels in the brain. Following microdialysis probe insertion into
185 hippocampus and a subsequent equilibration period to allow levels of ISF proteins stabilize, as
186 previously described[40,41], samples were collected over a baseline period before LPS treatment.
187 Samples were collected 10 hours following LPS and pre- and post-LPS period ISF samples were
188 quantified using an exploratory proximity extension assay (PEA)-based panel of cytokines,
189 chemokines, and related proteins (**Fig. 2h**). As shown in **Fig. 2i**, a number of expected pro-
190 inflammatory cytokines and chemokines were significantly elevated in the hippocampal ISF
191 following LPS treatment compared to the baseline period, including IL1β, CCL5, TNF, IL6, as well
192 as anti-inflammatory protein IL-10, which has been shown to be released by microglia following
193 LPS as a means to resolve the inflammatory response[42] (**Fig. 2i**). Having successfully dialyzed
194 and detected immune-related proteins using this method, we sought to assess the impact of
195 TIMP2 deletion on the hippocampal extracellular milieu. 2-3-month-old WT and KO mice were
196 subjected to the HMWCO *in vivo* microdialysis paradigm to sample hippocampal ISF during a
197 stable, steady state period of 24 hours prior to measurement of proteins from pooled ISF samples
198 (**Fig. 2j**). Interestingly, deletion of TIMP2 increased a number of proteins associated with
199 inflammation in the hippocampal ISF (**Fig. 2k)**, including chemokine CCL20 that we had found to
200 be elevated following LPS stimulation (**Fig. 2i**), and EDA2R, a member of the tumor necrosis
201 factor receptor superfamily whose levels correlates with increased age[43]. EDA2R cytokine
202 signaling contributes to inflammation through activation of the NF-κB pathway. TIMP2 deletion
203 also increased hippocampal ISF levels of HGF, a pleiotropic cytokine that modulates the

204 inflammatory response through NF-κB signaling that is also elevated in CSF of AD subjects[44,45].
205 Several proteins known to be upregulated under neurotoxic conditions as a means to limit damage
206 were also found to be upregulated in TIMP2 KO ISF, including EPO, GFRA1, TGFA[46,47], as was
207 the lysosomal serine protease TPP1 that is associated with phagocytic function[48,49]. As expected,
208 we also found that loss of TIMP2 increases hippocampal ISF levels of Matrilin-2 (MATN2), an
209 extracellular matrix (ECM) protein[25] that signals through TLR4 to induce proinflammatory genes
210 in macrophages to promote axonal damage[50]. Together, these changes in the hippocampal
211 extracellular environment may reflect a more pro-inflammatory, debris-rich environment relative
212 to that in WT hippocampus.
213
214 **Microglial TIMP2 regulates activation state**
215 Our findings suggest that loss of TIMP2 alters microglial activation and contributes to an
216 inflammatory extracellular environment, yet it remains unclear whether these differences are
217 mediated by the pool of TIMP2 produced by microglia, consistent with its expression pattern
218 demonstrated in our previous experiments (**Fig. 1b-c**). To explore the contribution of microglial
219 sources of TIMP2 to the microglial phenotypes associated with global TIMP2 deletion, we used a
220 TIMP2$^{fl/fl}$ model we generated[25] and crossbred them with *Cx3cr1*$^{CreERT2/+}$ mice[51] to inducibly delete
221 TIMP2 in *Cx3cr1*-expressing cells. Using a previously established adult microglia isolation
222 paradigm[52] (**Fig. 3a**) that successfully yielded pure adult microglia in culture (**Supplementary**
223 **Fig. 3a-c)**, we first induced Cre-mediated recombination and then confirmed efficient deletion of
224 microglial TIMP2 (**Supplementary Fig. 3d-e**). To examine how TIMP2 deletion in microglia
225 affects canonical activation marker expression, we imaged primary adult microglia expressing
226 CD68. Targeting microglial expression of TIMP2 significantly increased the number of cells
227 expressing CD68 (**Fig. 3b-c**). We also quantified the number of primary microglia expressing
228 senescent marker p16INK4a given the earlier pathway association in TIMP2 KO neonatal
229 microglia (**Supplementary Fig. 1h)**, which revealed a greater number of p16INK4a^{+} microglia

230 from *Cx3cr1*$^{CreERT2/+}$;*Timp2*$^{fl/fl}$ compared to that observed from *Timp2*$^{fl/fl}$ control mice. (**Fig. 3d-e**).
231 We next examined the number of IBA1^{+}CD68^{+} cells in the DG of 6-7 month-old
232 *Cx3cr1*$^{CreERT2/+}$;*Timp2*$^{fl/fl}$ or *Timp2*$^{fl/fl}$ control mice that had received tamoxifen (**Fig. 3f**). We
233 observed an increase in the extent of IBA1 staining covering the DG and an increase in the
234 number of activated microglia (IBA1^{+}CD68^{+}) (**Fig. 3f-h**). These findings suggest that removal of
235 the microglial pool of TIMP2 leads to microgliosis phenotypes that are consistent with those
236 observed in the setting of global TIMP2 deletion.
237
238 **Microglia contribute to external pools of TIMP2 and its removal modifies myelin**
239 **phagocytosis**
240 TIMP2 is present at high levels in the extracellular space of the hippocampus[25], likely reflecting
241 contributions from various sources, including from neurons and microglia. Our data show that
242 microglia express TIMP2 at both transcript and protein levels, yet it remains unclear whether
243 microglia release TIMP2, where it can potentially alter microglial response to pathological debris,
244 and whether targeting microglial TIMP2 affects associated phenotypes. To begin to explore these
245 questions, we isolated and cultured adult WT microglia to examine TIMP2 release into the media
246 across various timepoints in serum-free media, which was necessary given the high levels of
247 endogenous TIMP2 present in plasma/serum, especially at early life stages[16] (**Fig. 4a**).
248 Immunoblotting analysis on media from these cultures revealed that microglia release TIMP2 in
249 a time-dependent fashion (**Fig. 4b-c**). We then asked whether levels of TIMP2 released into the
250 media is modulated by exposure to various biological substrates (zymosan, 10 μg/mL; LPS, 100
251 ng/mL), including those commonly encountered within the brain (myelin, 10 μg/mL). 12 hours
252 following stimulation with these substrates, we measured TIMP2 levels in the conditioned media
253 by immunoblotting. While zymosan stimulation did not change TIMP2 levels in the media relative
254 to unstimulated conditions, LPS slightly increased levels, though this did not reach statistical

255 significance, and myelin stimulation robustly increased (~2-fold) TIMP2 release into the media
256 relative to unstimulated conditions (**Fig. 4d-e**).

257 Given that the brain accumulates abundant myelin debris with age[53], the increase in
258 TIMP2 in response to myelin stimulation motivated us to examine whether microglial TIMP2
259 modulates cellular response to myelin. We isolated adult microglia from tamoxifen-treated
260 *Cx3cr1*$^{CreERT2/+}$;*Timp2*$^{fl/fl}$ and *Timp2*$^{fl/fl}$ controls and performed a myelin phagocytosis assay in
261 which myelin was conjugated with pHrodo red, a pH-sensitive dye that fluoresces in the acidic
262 endosomal/lysosomal compartment that was monitored over time using a live-cell imaging system
263 (**Fig. 4f**)[54]. 'Area under the curve' analysis revealed significantly lower uptake of myelin in
264 *Cx3cr1*$^{CreERT2/+}$;*Timp2*$^{fl/fl}$ microglia over a 12-hour period compared to the uptake observed in
265 control microglia (**Fig. 4g-h**). We next assessed the rate of myelin clearance in the two groups by
266 treating new cultures with myelin, followed by withdrawal of the treatment with fresh media to
267 measure the rate of myelin elimination (**Fig. 4i**). We observed a lower rate of myelin clearance in
268 *Cx3cr1*$^{CreERT2/+}$;*Timp2*$^{fl/fl}$ microglia relative to Timp2$^{fl/fl}$ control microglia (**Fig. 4j-k**). Together, these
269 results suggest that deletion of microglial TIMP2 impairs microglial phagocytosis of myelin.

270 We previously reported that neuron-derived TIMP2 released into the brain extracellular
271 space is critical for hippocampal plasticity[25]. We next asked whether this additional extrinsic
272 source from neurons can regulate microglial state by creating Syn$^{Cre/+}$;*Timp2*$^{fl/fl}$ and *Timp2*$^{fl/fl}$ mice
273 to target neuronal TIMP2 expression[25] and then performing confocal imaging to evaluate
274 microglial state using IBA1 and CD68 markers (**Fig. 4l**). Similar to our findings demonstrating that
275 targeting the microglial pool of TIMP2 affects microglial state (**Fig. 3h**), we find that neuronal
276 TIMP2 deletion significantly increases the number of IBA1^{+}CD68^{+} cells in the DG (**Fig. 4m-n**),
277 while the total number of microglia in this region was not affected by TIMP2 deletion
278 (**Supplementary Fig. 4a-b**). Together, our findings indicate that microglia are responsive to
279 modulation of extracellular levels of TIMP2, regardless of whether the source is from microglia or
280 neurons.

281

282 **Systemic TIMP2 treatment reduces age-associated microgliosis and modulates microglial**
283 **state**

284 Given our data suggesting that extrinsic sources of TIMP2 regulate microglial state *in vivo*, we
285 next asked whether extrinsic application of TIMP2 to aged primary microglia could directly affect
286 microglial state phenotypes observed in our KO models, independent of regulation from other cell
287 types. We first isolated microglia from 20-month-old WT mice and evaluated whether application
288 of TIMP2 altered the number of IBA1$^+$CD68$^+$ cells in the culture (**Fig. 5a**). Treating aged primary
289 microglia with TIMP2 reduced the number of CD68$^+$ cells relative to control conditions (**Fig. 5b-**
290 **c**), suggesting that TIMP2 can directly alter microglial state independent of its known effects on
291 other CNS cell types[23,25,55]. Based on our previous results demonstrating that TIMP2 enters the
292 brain from blood following systemic injection[16], we next asked whether systemic treatments with
293 TIMP2 in aged mice can regulate microglial state and function. Using the same dosing paradigm
294 we previously showed improves learning and memory in aged mice (**Fig. 5d**)[16], we injected aged
295 WT mice systemically with TIMP2 (50 μg/kg), and isolated brains to evaluate changes in microglia
296 after ~2.5 weeks of injections. Systemic TIMP2 treatment reversed the consistent increase in
297 microglial activation observed in our KO models, as reflected by the decreased number of
298 IBA1$^+$CD68$^+$ cells in the DG of TIMP2-treated aged mice compared to vehicle-treated aged mice
299 (**Fig. 5e-f**). We also detected a lower percentage of DG area occupied by CD68 staining, whereas
300 the treatment did not affect the total number of IBA1$^+$ cells (**Supplementary Fig. 5a-c**).

301 To characterize how aged microglia respond to TIMP2 treatment at the transcriptomic
302 level, we applied a single-nuclei RNA-sequencing (snRNA-seq) pipeline on hippocampi isolated
303 from a new cohort of vehicle- and TIMP2-treated 20-month-old mice, based on an established
304 method[56]. Following quality-control measures to remove ambient RNA, doublets, and poor-quality
305 nuclei, we obtained 60,436 nuclei for downstream analysis in which nuclei from each sample were
306 integrated and clustered using uniform manifold approximation and projection (UMAP)

307 (**Supplementary Fig. 5d**). Combining use of ScType for automated cell-type identification[57] and
308 thorough interrogation of top marker genes for each cluster, we identified CNS cell types expected
309 for the hippocampus (**Supplementary Fig. 5d-e**). We next subclustered cells identified as
310 microglia (2,831 nuclei; **Fig. 5g**) and noted significant shifts in the proportion of cells in subclusters
311 2, 5, and 6 in mice treated systemically with TIMP2 compared to vehicle-treated mice (**Fig. 5h**;
312 **Supplementary Fig. 5f**). To identify what processes characterize these TIMP2-shifted
313 subclusters, we performed IPA on the significant genes defining these subclusters and examined
314 expression levels of top marker genes. TIMP2 treatment increased the proportion of microglia in
315 subcluster 2, a cluster characterized by the highest expression of *Apoe,* a gene that regulates
316 phagocytosis and lipid uptake[28,58] (**Supplementary Fig. 5g**), as well as by iron handling ("uptake
317 and transport") and immune response processes ("cyclophilin signaling") (**Fig. 5i**). TIMP2
318 treatment shifted subcluster 1, albeit modestly (**Supplementary Fig. 5f**), which was characterized
319 by genes relating to phagosome formation and signaling in myeloid cells (**Supplementary Fig.
320 5h**). TIMP2 treatment significantly increased the proportion of microglia in subcluster 5 (**Fig. 5h;
321 Supplementary Fig. 5f**), a cluster defined by "axon guidance signaling", "synaptogenesis
322 signaling", and "neurexins and neuroligins" (**Fig. 5j**). This subcluster, along with 2 other microglial
323 subclusters with neuron-associated genes, also had highly enriched expression of *Gria1*
324 (**Supplementary Fig. 5g**), a gene linked to microglial-neuron interactions[59,60]. Intriguingly, we
325 found that TIMP2 treatment resulted in a significant decrease in proportion of subcluster 6
326 microglia (**Fig. 5h; Supplementary Fig. 5g**), which were defined by pathways associated with
327 production of "nitric oxide and reactive oxygen species (ROS) in macrophages", "senescence",
328 "Fcγ receptor-mediated phagocytosis", "IL-3, IL-5, and GM-CSF signaling", and "HGF signaling"
329 (**Fig. 5k)**. Further analysis of subcluster 6 markers revealed "TNF" as a top upstream regulator
330 (**Fig. 5l**), activating proinflammatory[61-63] and senescence-associated[64] pathways through IL6,
331 IFNG, STAT1/STAT5A, IRF8, and TP53, as well as IL10 as a counter-regulatory response

332 protein[65], together suggesting that TIMP2 treatment of aged mice reduces the proportion of
333 microglia associated with a pro-inflammatory and senescent-like state.

334 Given these shifts in microglial subclusters following TIMP2 treatment, we next aimed to
335 compare overall microglial gene expression changes following TIMP2 treatment. We found that
336 TIMP2 treatment resulted in differentially expressed genes (DEGs; 196 upregulated, 68
337 downregulated) in the overall microglia cluster. *Cst3* and *Apoe* were the two most significantly
338 upregulated genes (**Fig. 5m**). *Apoe* is a well-characterized regulator of the DAM transcriptional
339 state[28] and is upregulated in microglia phagocytosing apoptotic neurons[58], while *Cst3* is localized
340 in the lysosome, where it regulates lysosomal homeostasis[66]. We also observed a change in
341 ferroptosis-associated *Fth1*[67] and genes linked to metabolism and inflammation, including
342 *Ndufa4*[68] and *Tmsb4x,* which negatively regulates NFκB signaling[69] (**Fig. 5m**). Pathway analysis
343 on the overall DEGs reflected changes in cytokine/chemokine and interferon signaling, as well as
344 altered uptake processes (ferroptosis), and potential changes in microglia-neuron interactions
345 (ERBB4 and ERBB2 signaling) (**Fig. 5n**). We performed pre-ranked Geneset enrichment analysis
346 (GSEA)[70] to determine if genes, ranked by signed fold-change*-$\log_{10}$*P*-value$_{adj}$, were enriched
347 within gene sets previously associated with different microglial states, including disease-
348 associated microglia (DAM)[28], lipid-associated macrophages (LAM)[71], which was identified as a
349 protective state in adipose tissue of mice on a high-fat diet[71], lipid-droplet-accumulating microglia
350 (LDAM)[12], activated response microglia (ARM)[72], interferon-related[73] and homeostatic microglia[72].
351 Interestingly, we found that TIMP2 treatment resulted in positive enrichment in LAM, DAM, and
352 ARM gene sets in microglia (**Fig. 5o; Supplementary Fig. 5i**), supporting a putative enrichment
353 in genes associated with protective response to damage.

354

355 **Systemic TIMP2 restores phagocytic capacity in aged microglia**

356 Phagocytic capacity of microglia is diminished in aging and in proinflammatory states[8,9,74], and
357 targeting this process may facilitate effective clearance of dead cells or debris[9,10,75]. Given the

358 TIMP2-induced changes observed in microglial phagocytosis-related pathways and in putative
359 microglial-synapse interactions in snRNA-seq experiments, we evaluated how systemic TIMP2
360 treatment affects the ability of microglia to phagocytose synaptic content in the DG. We
361 hypothesized that TIMP2 treatment restores microglial phagocytosis in aged DG, especially given
362 our results showing that microglia-specific *Timp2* deletion reduced myelin phagocytosis (**Fig. 4g-**
363 **h**). To evaluate phagocytosis in aged mice following TIMP2 or vehicle treatment (**Fig. 5d**), we
364 performed confocal imaging of sections stained with antibodies for IBA1, CD68, and synaptic
365 marker VGLUT1, followed by Imaris-3D reconstruction to visualize lysosome-associated synaptic
366 puncta in individual microglia. We found that TIMP2 treatment increased the volume of VGLUT1^{+}
367 puncta within microglia lysosomes in the DG relative to vehicle treatment (**Fig. 5p-q**), reflecting
368 enhanced phagocytic function of a process typically diminished with aging.
369

370 **Discussion**

371 Here, we define a novel role of youth-associated protein TIMP2 in regulating microglial state in
372 the context of aging pathology and in normal brain homeostasis. Global, microglial-specific, and
373 neuronal-specific deletion of TIMP2 accelerated activation and associated deleterious
374 phenotypes of microglia in the hippocampus. TIMP2 also appeared to modulate the phagocytic
375 uptake and clearance of physiological substrates by microglia, including myelin, while regulating
376 the inflammatory state of these cells. Given that various sources of expression contribute to the
377 brain extracellular pool of TIMP2, we explored how systemic supplementation with TIMP2 in aged
378 mice affects microglia, which reversed many of the phenotypes associated with TIMP2 removal,
379 including microgliosis and impaired phagocytosis, while highlighting transcriptomic shifts in
380 microglia associated with deleterious microglial phenotypes. Together, our results highlight that
381 microglia are sensitive to extracellular levels of TIMP2, and that increasing TIMP2 promotes a
382 shift toward a more protective state that may counteract age-associated pathology.

383 Early studies provided intriguing evidence that exposure to the systemic environment
384 affects microglia[18,76] and that these cells subsequently take up proteins originating in plasma[20,21],
385 yet little is known of the effects of such proteins on microglia. Specifically, recent work found that
386 labeled plasma proteins are found within microglia of healthy brains in a process that appears to
387 involve a specialized subset of microglia characterized by antigen presentation, as well as high
388 metabolic and phagocytic activity[21], though it remains unclear whether these processes diverge
389 in the aged brain. A further recent study identified PF4 as a blood-borne factor that modulates
390 microglial state, though it may not penetrate the brain appreciably and instead acts on peripheral
391 T cells to indirectly modulate the CNS[18,77], highlighting that microglia likely respond to blood-borne
392 factors through a variety of mechanisms. In the case of TIMP2, previous work found that labeled
393 TIMP2 enters the brain after peripheral delivery in aged mice[16]. Our current data examining the
394 impact of neuronal, microglial, and systemic sources of TIMP2 on microglial phenotypes
395 collectively support the concept that extracellular pools of TIMP2 regulate microglial function.

396 A growing literature has highlighted roles for TIMP2 in regulating overall hippocampal
397 function by modulating synaptic plasticity mechanisms[16,25], raising the possibility that some of the
398 effects observed in microglia may reflect, in part, its action on neurons. While this remains a
399 possibility, we find that aged primary microglia treated with TIMP2 recapitulate phenotypes
400 observed in the intact brain when aged mice are treated systemically with TIMP2, suggesting that
401 microglia are directly responsive to TIMP2. In terms of its molecular targets, a recent study using
402 a modified TIMP2 construct lacking MMP inhibitory activity was still sufficient to enhance
403 hippocampal plasticity phenotypes, arguing for non-canonical targets for TIMP2 activity[23] beyond
404 classical interactions with MMPs. Given the many distinct interactions for TIMP2 activity that have
405 been identified[24], future studies should focus on delineating molecular targets for specific CNS
406 functions.

407 To further examine how TIMP2 modulates microglial state, we applied a combination of *in*
408 *vivo* and *in vitro* approaches across multiple ages, which revealed a consistent phenotype of

409 heightened microglial activation in the setting of TIMP2 deficiency that is reversed with TIMP2
410 supplementation. To characterize the local extracellular environment, we implemented an *in vivo*
411 microdialysis method that permitted sensitive assessment of immune-related proteins, an
412 approach that revealed marked alterations in the extracellular milieu in factors related to
413 inflammation, lysosomal activity, and cellular stress responses, reflecting altered
414 neuroinflammatory environment. Our transcriptomic analysis of aged microglia from TIMP2-
415 treated mice largely corroborated these roles of TIMP2 as a driver of protective microglial states.
416 In microglia of aged mice treated with TIMP2, we find enrichments in sets of genes resembling
417 the LAM[71], DAM[28], and ARM[72] states associated with protective macrophage/microglia function.
418 DAM and ARM states are both associated with protective responses to aging and AD
419 pathology[28,72] while being characterized by elevated *Apoe* expression, a top upregulated gene in
420 TIMP2-treated microglia in our dataset. Several studies have demonstrated that these states, and
421 induction of genes associated with these states, are necessary for microglia to appropriately
422 respond to damage[28,58,72,78,79]. We also found significant enrichment in the LAM geneset in TIMP2-
423 treated microglia, which has been argued to be a protective myeloid state in adipose tissue of
424 mice on a high-fat diet[71]. These macrophages are involved in phagocytosis, lipid catabolism, and
425 energy metabolism[71], largely fitting with our observed upregulation of genes related to
426 phagocytosis, metabolism, and modulation of inflammatory response in microglia from TIMP2-
427 treated mice. The enrichment in genes associated with LAM, DAM, and ARM states with TIMP2
428 treatment may reflect a shared change in microglial response to lipid-rich damage, including the
429 myelin debris encountered by aged microglia, possibly a protective response to aging that is
430 bolstered with TIMP2 treatment. Corroborating the protective effects, we see a corresponding
431 loss of microglial subpopulations characterized by deleterious pathways in microglia from TIMP2-
432 treated mice, including senescence, production of nitric oxide and ROS, and pro-inflammatory
433 programs driven by TNF. A previous *in vitro* study using the BV2 cell line suggested that TIMP2

434 may have anti-inflammatory roles, including production of IL10 and reduction of pro-inflammatory
435 cytokines following LPS stimulation[80], supporting our *in vivo* observations.

436 A consistent phenotype we observed across experiments modulating TIMP2 levels is the
437 shift in microglial activation and associated lysosomal and phagocytic capacity. Using lysosomal-
438 associated marker CD68, we show that removing TIMP2 increases activation state, while
439 reducing uptake and removal of myelin, together supporting that TIMP2 regulates how
440 physiological material is removed from the extracellular space. Interestingly, by sampling the brain
441 extracellular space of mice lacking TIMP2, we detected elevations in the lysosomal serine
442 protease TPP1, perhaps reflecting response to aberrant debris removal by microglia, a
443 phenomenon observed under conditions of lysosomal stress[81,82]. Conversely, TIMP2 treatment of
444 aged mice reduces microglial activation and increases phagocytic capacity—a function typically
445 diminished with age and under proinflammatory conditions[8,9,74]. These data dovetail with our
446 transcriptomic data from treated aged mice that reveal upregulation of genes involved in
447 phagocytic processes and metabolism and a shift away from proinflammatory microglial states,
448 perhaps reflecting a more efficient endolysosomal capacity. In addition to the benefit of clearing
449 debris to protect the local brain environment, the process of phagocytosis itself can also inhibit
450 proinflammatory responses[83], though future work will need to identify the directionality of these
451 changes following treatment with TIMP2 and related factors. Together, this work suggests that
452 TIMP2 modulates the ability of microglia to remove extracellular material, enabling them to more
453 effectively engage in phagocytosis while reducing the inflammatory environment in the setting of
454 age-related pathology.

455

456 Our findings demonstrate that TIMP2 modulates microglial state, enhancing phagocytic function
457 and dampening inflammatory activation in the aged brain. By promoting a more protective set of
458 microglial phenotypes, TIMP2 may help counteract accumulation of debris and chronic
459 inflammation that characterize the aged CNS environment. Given that genetic risk for AD is

460 enriched in genes involved in microglial phagocytosis and endolysosomal function[84], future
461 studies should explore how TIMP2 influences these pathways in contexts of aging and age-
462 related neurodegenerative conditions. Together, our work positions TIMP2 as a promising
463 candidate for mitigating microglial dysfunction and preserving brain health across the lifespan.

464 **Materials and Methods**

465

466 **Animals**

467 Animal procedures, care, and handling were performed in accordance with the NIH Guide for
468 Care and Use of Laboratory Animals and the Icahn School of Medicine at Mount Sinai Institutional
469 Animal Care and Use Committee. All mice were maintained on C57Bl/6 background. TIMP2 -/-
470 (KO) mice were purchased from Jackson Laboratory, and 5xFAD mice were purchased from
471 MMRRC and subsequently maintained in-house alongside WT littermates. *Timp2*$^{fl/fl}$ mice were
472 generated as previously described[25] and crossbred with *Cx3cr1*$^{CreERT2/+}$*Lit51t* mice or Syn$^{Cre/+}$ lines
473 (Jackson) to permit microglial and neuronal deletion[25] of TIMP2, respectively. To induce
474 conditional deletion of microglial *Timp2*, 2-month-old mice were administered 100 mg/kg
475 tamoxifen (Sigma Aldrich Fine Chemicals Biosciences, T5648) in corn oil (Sigma, C8267) 5 times
476 by oral gavage, with at least 48-h separation between gavages[78]. Cre-negative *Timp2*$^{fl/fl}$
477 littermates were also given tamoxifen as controls. Aged WT C57BL/6 mice were obtained from
478 the National Institute on Aging aged rodent colony. Male and female mice were used unless
479 otherwise indicated.

480

481 **Neonatal microglia isolation**

482 Using an established protocol[85], we dissected forebrain from pups (P5-P8) and manually
483 homogenized the tissue using a dounce homogenizer (VWR, KT885300-0002), prior to debris
484 removal using a 20% Percoll gradient (GE Healthcare, 17-0891-02). Microglia were positively
485 selected using CD11b microbeads (Miltenyi Biotec, 130-049-601), LS columns (Miltenyi Biotec,
486 130-042-401), and a QuadroMACS Separator according to manufacturer instructions. For
487 western blot analysis, cell pellets were collected and frozen at -80C until use. For ICC and bulk
488 RNAseq experiments, cells were manually counted with a hemacytometer and Trypan blue
489 staining to assess cell viability. Cells were plated at a density of 200,000 microglia/well in 96-well

490 poly-d-lysine-coated plates (Corning, 354461) in Dulbecco's modified Eagle's medium (DMEM)
491 supplemented with 10% FBS (Sigma, F4135, Sigma) and 1% penicillin–streptomycin (Gibco,
492 15140). Microglia recovered for a minimum of 2 days in tissue culture incubator before
493 experiments.
494
495 **Adult microglia isolation**
496 Following an established protocol[52], mice were perfused with ice-cold PBS, cerebellum and
497 olfactory bulbs were removed, and remaining brain tissue was enzymatically dissociated using
498 the Neural Tissue Dissociation Kit (P) (Miltenyi Biotech, 130-092-628) according to manufacturer
499 instructions. During incubation in enzymatic buffer, large, medium, and small fire polished Pasteur
500 pipettes were used to mechanically dissociate tissue. Following filtration and centrifugation,
501 samples were incubated with CD11b microbeads (Miltenyi Biotec 130-049-601) and subsequently
502 separated using LS columns (Miltenyi Biotec 130-042-401) and QuadroMACS Separator using
503 manufacturer's instructions. Cells were plated on imaging plates (Cellvis, P96-1.5H-N) or poly-L-
504 Lysine-coated glass coverslips (Electron Microscopy Sciences, 72292-04) in DMEM
505 supplemented with 10% FBS and 1% penicillin–streptomycin. Microglia were allowed to recover
506 for 7 days in a tissue culture incubator before experiments. Wells were excluded from analysis if
507 cultures did not meet viability or quality control criteria (e.g. excessive debris).
508
509 ***In vitro* phagocytosis assay**
510 Following a 7-day recovery period post-isolation, conditioned media from primary microglial
511 cultures was removed and replaced with serum-free media before measurements in the IncuCyte
512 S3 live-cell analysis system (Sartorius) that contained a tissue culture incubator at 37C/5% CO2
513 for baseline imaging. Cells were treated with pHrodo-labeled myelin[54] (10 μg/mL), generously
514 provided by the laboratory of Dr. Alison Goate, and imaged hourly at 20x using phase contrast
515 and red fluorescent signal. For myelin clearance experiments, following a 3-hour incubation with

516 pHrodo-labeled myelin, cells were washed with PBS and fresh serum-free media was added that
517 did not contain myelin. Total integrated density was calculated by multiplying the average red
518 object mean intensity (RCU, red calibrated units) by the average phase object area (cell, μm^2)
519 and plotted over time[86]. For both uptake and clearance experiments, two independent
520 experiments were conducted with 3 technical replicates per animal that were averaged.
521

522 ***In vitro* microglial stimulation**

523 To assess TIMP2 secretion with various substrates, cultures of adult WT microglia were
524 stimulated with various substrates in serum-free media at the following concentrations: Zymosan
525 10 μg/mL, myelin 10 μg/mL, LPS 100 ng/mL, or PBS control. 12 hours following stimulation,
526 conditioned media was collected and concentrated for immunoblotting. For experiments
527 examining activation of primary microglia from aged mice following TIMP2 treatment, cell media
528 was replaced with serum-free media 2 hours prior to incubation with TIMP2 (2 μg/mL, R&D
529 Systems, 6304-TM-010) or vehicle (PBS) for 28 hours, after which cells were fixed and stained to
530 evaluate markers.
531

532 **Bulk RNA-sequencing of neonatal microglia**

533 Forebrains from neonatal mice were pooled by genotype, and then microglia were isolated and
534 plated in 12-well poly-d-lysine-coated plates (Corning, 354470) at a density of 600,000 cells per
535 well, 2 wells per genotype. After 72 hours, trypsin was used to remove cells prior to centrifugation
536 for 5 minutes at 1230 x g, followed by resuspension in PBS, and re-centrifugation. Pellets were
537 stored at -80C before further processing and sequencing by Genewiz (Azenta) with each sample
538 representing independent isolations from pooled pups. RNA was extracted and quality was
539 measured using TapeStation Analysis Software 3.2 (Agilent), and concentration was determined
540 using Qubit assay, with all samples exhibiting RNA Integrity Number (RIN) = 10. Sequencing

541 libraries were prepared with poly(A) selection and sequenced using Illumina Hiseq (2x150bp
542 paired-end) according to manufacturer protocols. Reads were mapped to the Mus musculus
543 GRCm38 genome. Differential expression was performed using DESeq2, and differentially
544 expressed genes (P<0.05) were used to perform Ingenuity Pathway Analysis (IPA, Qiagen), as
545 well as gene ontology over-representation analysis with the MSigDB[31] database on significantly
546 upregulated and downregulated genes separately.
547
548 **Immunoblotting**
549 To perform western blot analysis of TIMP2 in primary microglia, cell pellets from pooled samples
550 were lysed in RIPA buffer (Thermo Fisher) containing protease Inhibitor cocktail (Roche) for 30
551 min on ice, collecting lysates following a 30-min centrifugation at 15,000 x g. 80 μg of protein per
552 sample was loaded on Bolt 4-12% Bis-Tris Plus Gels (Invitrogen). TIMP2 from conditioned media
553 was spun at 1,000 x g for 10 min to remove debris. Protease inhibitor cocktail was added to
554 supernatant prior to concentration of media by centrifugation at 4,000 x g for 40 min using Amicon
555 Ultra-15 centrifugal filter unit (Amicon, UFC901024) before loading on 4-12% NuPAGE Bis-Tris
556 denaturing gels (Invitrogen). Gels were transferred, the blots probed with anti-TIMP2 (1:5000;
557 D18B7, Cell Signaling) or anti-actin (1:10000; A5060; Sigma), and then developed as previously
558 described[25]. Band intensities were quantified using ImageJ software as described[41].
559
560 **Immunocytochemistry**
561 Following fixation with 4% paraformaldehyde for 20 min at room temperature, primary microglia
562 were washed three times with PBS, incubated with blocking solution (10% donkey serum and
563 0.1% triton-X in PBS) for 1 hour, and then incubated overnight at 4C with primary antibodies in
564 blocking solution at the following concentrations: IBA1, 1:500, (019-19741, Wako); CD68, 1:200,
565 (MCA1957, BioRad), TIMP2, 1:100 (AF971, R&D systems, [2-day incubation]), p16INK4a, 1:500,
566 (MA5-17142, Invitrogen). Cells were then washed and incubated in their corresponding secondary

567 antibody for 1 hour. Staining was visualized and imaged using the Keyence BZ-X700 microscope
568 or Zeiss LSM780 upright confocal microscope using a 40x objective. 2-3 wells per mouse were
569 plated and 3-4 images per well were averaged for 3 technical replicates per mouse. The value for
570 each mouse represents the mean of these replicates.
571
572 **Immunohistochemistry and imaging**
573 Following anesthetization with a ketamine (90 mg/kg) and xylazine (10 mg/kg) cocktail, mice were
574 perfused transcardially with ice-cold 0.9% saline. Brains were dissected and postfixed in 4%
575 paraformaldehyde for 48 hours and then preserved with 30% sucrose in PBS. 40-μm sections
576 were prepared from hemibrains and sectioned using a freezing-sliding microtome and stored at -
577 20C in cryoprotectant media prior to immunohistochemistry according to our previous protocol[16].
578 Briefly, free-floating sections were blocked in appropriate serum (10%) before incubation in
579 primary antibody at 4C overnight. Primary antibodies were used at the following concentrations:
580 IBA1, 1:500, (Wako, 019-19741); CD68, 1:200, (MCA1957, BioRad); VGLUT1, 1:2000, (135318,
581 Synaptic Systems); CD68, 1:500, (137001, BioLegend, paired with IBA1 and VGLUT1 co-
582 staining). Sections were then incubated in the corresponding fluorescently-conjugated secondary
583 antibodies for 1 hour (1:200 in TBST), followed by DAPI, where indicated, for 15 min. Stained
584 sections were mounted and coverslipped with ProLong Gold (Invitrogen).
585 To image staining in the dentate gyrus, 2x2 tile-scanning images were acquired through
586 the entire z-plane of sections (1-μm intervals across ~40μm) at 40x/1.4 oil DIC objective using a
587 Zeiss LSM780 upright confocal microscope. For all imaging experiments, 3-4 sections per animal
588 were imaged according to stereological principles, as previously described[16]. FIJI was used to
589 perform thresholded "percentage area" or count analysis of cells expressing CD68 and/or IBA1
590 across mouse experiments in a blinded fashion. Count data was normalized to the area of the
591 analyzed ROI.
592 *Imaris-based imaging and analysis*

593 Following IHC for VGLUT1, IBA1, and CD68, images containing dentate gyrus were acquired
594 using a 63X oil-immersion objective lens on a Zeiss LSM780 with 0.33-μm z-step size across ~20-
595 μm z-stack (1024x1024 pixels). 3D reconstruction of microglia was performed using Imaris (Imaris
596 10.2, Oxford Instruments). Microglial surfaces were created using machine learning-based
597 training on the IBA1 channel, which were then used to mask the CD68 channel. A surface was
598 then created for the microglial-masked CD68 and used to mask VGLUT1 signal. A surface for
599 VGLUT1 signal within a microglial lysosome was created, together creating $VGLUT1^+$ surfaces
600 within a microglial lysosome. The total volume of VGLUT1 within lysosomes was normalized to
601 the volume of the microglial surface analyzed. Three sections per mouse were imaged, and
602 results for microglia were averaged to represent a value for each mouse. A total of 44-47 microglia
603 were analyzed per group.

604 *Microglia morphology analysis*

605 We employed an established protocol defining microglia morphologies based on their circularity
606 ($(4\pi \text{ Area}) / \text{Perimeter}^2$) assessed by FIJI, where values approaching a value of 1 approximate a
607 circular morphology[33-36]. "Ramified" morphology was categorized according to circularity between
608 0 and 0.400, "activated/reactive" microglia are defined by circularity of 0.500-0.699, and
609 "ameboid" morphology are defined by circularity of 0.700-1.000. Images were imported to FIJI,
610 converted to 8-bit, background-corrected (rolling ball radius of 50 pixels and despeckled) equally
611 across images/groups, and then classified into the three morphology types according to
612 circularity. The number of microglia corresponding to each morphology class was normalized to
613 stereologically-defined dentate gyrus areas.

614

615 **Recombinant protein injections**

616 For experiments in which mice were treated systemically with TIMP2, aged mice were given
617 intraperitoneal (i.p.) injections every other day with either vehicle (PBS) or recombinant mouse

618 TIMP2 (R&D Systems, 6304-TM-010) for a total of 8 injections, using our established protocol, a
619 method used previously to provide revitalization of hippocampal plasticity and cognitive function[16].
620
621 **Nuclei Isolation and snRNA-seq**
622 Full hippocampi were isolated, flash-frozen, and stored at -80C until processing. Hippocampi were
623 thawed on ice, and nuclei were isolated using established protocols[56]. Briefly, each hippocampi
624 was mechanically dissociated using a dounce homogenizer (VWR) with 2 ml of EZ lysis buffer
625 (Millipore Sigma). Samples were centrifuged, resuspended in fresh lysis buffer, and centrifuged
626 again. Cell pellets were gently washed with 4 ml ice-cold PBS, and supernatant were removed
627 prior to resuspending pellets in 100 µl of ice-cold PBS with 0.04% BSA (NEB) and 1 U/µL RNAse
628 inhibitor (Millipore Sigma). Each sample was filtered through 40-µm FlowMi cell strainers
629 (Millipore), and nuclei were counted (aided by trypan blue) to assess nuclei viability using an
630 EVOS M7000. Two biological samples from the same treatment condition were pooled to load
631 20,000 nuclei total (10,000 nuclei each) for a total N=2 samples per treatment condition. Libraries
632 were prepared and sequenced by the Single-cell & Spatial Technologies Team, Center for
633 Advanced Genomics Technology Genomics Core (ISMMS) using the 10x Genomics Chromium
634 platform for library preparation (V2 3' GEX protocol) according to manufacturer's instructions.
635 Briefly, cDNA was extracted from Gel-Bead in Emulsions (GEMs) obtained from the sample chip
636 in the Chromium controller, and library quality control was performed with MiSeq Nano. Libraries
637 were run on Illumina NovaSeq 6000 S4 Flowcell (2x100 nt paired-end read length) configuration,
638 targeting 50,000 reads per cell.
639 Raw read data was analyzed by 10x Cell Ranger (v7.1.0) to align to reference genome
640 (Mus musculus, version mm10 2020-A). Downstream processing was performed in the R
641 programming environment (v4.2.0 or v4.4.2). Ambient RNA was removed from samples using
642 SoupX[87] and manual application of a stringent contamination fraction on a per sample basis. After
643 initial filtering, doublets were identified and removed using DoubletFinder[88]. Further filtering

644 involved removing genes expressed in fewer than 3 cells, cells with a UMI count under 500, and
645 cells with only 500 genes per cell to ensure we analyzed high-quality cells. The Seurat object was
646 then log-normalized, and variable features were identified using the FindVariableFeatures
647 function. ScaleData was then used to regress cells with more than 2% mitochondrial, ribosomal
648 large subunit (RPL) and ribosomal small subunit (RPS) gene expression content. Using STACAS,
649 a semi-supervised data integration method, we integrated all samples[89], which was used for cell
650 clustering. Using Seurat (v5.2.1), integrated samples were scaled, and clusters were identified
651 using FindNeighbors (using top 50 principal components) and FindClusters (Resolution=0.25). To
652 identify markers of each cluster, the RNA assay was processed using NormalizeData,
653 FindVariableFeatures, ScaleData (regressing out > 2% mitochondria, RPS, and RPL), and
654 FindMarkers. We determined cluster identity by assessing the top 30 markers on DropViz, further
655 confirming identities with ScType[57] and by examining literature-based expression of marker genes
656 for each cell type. Clusters identified to be microglia were subclustered (using the top 15 principal
657 components and a resolution of 0.5). Clusters suspected as containing doublets, i.e., marked by
658 high nCount_RNA and nFeature_RNA, as well as a lack of microglial genes as cluster markers,
659 were removed, and the remaining cells were re-clustered using the top 15 principal components
660 and a resolution of 1. Pathways representing each subcluster were evaluated using the
661 significantly upregulated marker genes in each subcluster ($P_{adj} < 0.05$; via FindAllMarkers) and
662 by running these markers in Ingenuity Pathway Analysis (IPA, Qiagen) and gene ontology over-
663 representation analysis using MSigDB[31]. To compare shifts in the proportion of subclustered cells
664 between treatment conditions, we employed scProportionTest[90].

665 Differential gene expression analysis for the microglia cluster was conducted using
666 DESeq2, and IPA was run on significant genes ($P_{adj} < 0.05$). After removing genes not mapping
667 to Entrez identifiers, we performed GSEA using a ranked list of all genes tested in the differential
668 expression analysis to assess enrichment in published gene sets representing characterized
669 microglial states[70]. GSEA was performed in R using the clusterProfiler[91] package (v4.14.6),

670 implementing the Fast GSEA (fgsea) algorithm with default parameters[92]. The Benjamini-
671 Hochberg correction method was applied to adjust for multiple comparisons for differential
672 expression and pathway analyses.
673
674 **1-MDa *in vivo* microdialysis**
675 Stereotaxic surgery and 1-MDa *in vivo* microdialysis was performed as previously described[25].
676 Mice were anesthetized with 2% isoflurane, and the head was shaved and fixed in a stereotaxic
677 apparatus (Stoelting Co.). Skull position was leveled, and a hole was drilled at bregma -3.1 mm,
678 2.5 mm lateral to target the left caudal hippocampus. Another hole was made diagonal to the first
679 to position an anchoring bone screw. After meninges were removed, an AtomosLM Guide
680 Cannula (PEG-12, Eicom) was inserted at a 12° angle, 1.2 mm below the brain surface at the
681 target location. The cannula was secured, and skin was closed using dental cement and surgical
682 adhesive glue. An AtmosLM Dummy Cannula (PED-12, Eicom) was inserted into the guide
683 cannula and secured with a plastic cap nut as the animal recovered in a clean cage on a heating
684 pad. Approximately 12 hours following surgery, 1-MDa *in vivo* microdialysis probes (AtmosLM;
685 Emicon) were inserted into caudal hippocampus. To calibrate the system prior to probe insertion,
686 inlet tubing (FEP tubing 0.65 mm OD x 0.12 mm ID, BASi) was connected to a syringe pump
687 (KdScientific) that perfused artificial cerebrospinal fluid (aCSF) containing, in mM: 1.3 $CaCl_2$, 1.2
688 $MgSO_4$, 3 KCl, 0.4 KH_2PO_4, 25 $NaHCO_3$, 122 NaCl, pH 7.35, at a rate of 1.2 µl/min. The outlet
689 tubing was connected to a peristaltic pump (MAB 20, SciPro), which was carefully calibrated to
690 obtain a pull rate between 0.9-1.1 µl/min. Probe integrity was tested, and once passing initial
691 quality control, it was connected to the inlet and outlet ports. The push-pull system was connected
692 to the probe and allowed to equilibrate prior to implanting in mouse brain. The probe was secured
693 with a cap-nut, and mice were placed in a Raturn (Stand-Alone Raturn System, BASi) and
694 tethered by a loose collar to enable free movement while preventing tangling of microdialysis
695 tubing. Dialysate from brain ISF was collected hourly at ~1.0 µl/min into a refrigerated fraction

696 collector (MAB 85 Fraction Collector, SciPro) and frozen at −80°C after collection for pooling and
697 subsequent measurement. In microdialysis experiments involving LPS administration, mice were
698 given a single i.p. injection of LPS (5 mg/kg in PBS), and samples were collected for an additional
699 10hrs. For all experiments, mice were given *ad libitum* access to food and water and were kept
700 under constant light conditions to minimize the impact of circadian protein flux, as previously
701 described[93].
702
703 **Protein analysis from ISF dialysates**
704 Hippocampal ISF dialysate samples were thawed on ice and pooled for measurements. For WT
705 and TIMP2 KO comparisons, samples representing the stable 24-hour steady-state period were
706 pooled within each mouse for subsequent measurements. For LPS experiments, the period
707 representing a stable baseline over a 12-hour period were pooled within each mouse to serve as
708 the pre-LPS sample per mouse. Samples corresponding to hours six to ten following LPS
709 treatment were pooled within each mouse to serve as the post-LPS treatment samples per
710 mouse. For all experiments, 230 µl of pooled sample was concentrated approximately 6-fold by
711 centrifugation at 14,000 x g for 75 min at 4C with a concentrator unit (Amicon Ultra-0.5 Centrifugal
712 Filter Units (MilliporeSigma). 25 µl of concentrated sample was loaded on a 96-well plate using
713 the Olink Target Mouse Exploratory Panel, encompassing cytokines and chemokines (Olink,
714 Uppsala Sweden) in coordination with the Human Immune Monitoring Center (ISMMS). Data was
715 represented as Normalized Protein EXpression (NPX) unit on a log2 scale.
716
717 **Statistical analysis**
718 Statistics were performed using GraphPad Prism version 10 (GraphPad Software) or R
719 programming environment (version 4.4.2 or version 4.2.0) using tests described in figure legends.
720
721 **Acknowledgements**

We would like to thank Anna Podlesny-Drabiniok, Michael Sewell, Raphael Kubler, and Mikaela Rosen for advice related to snRNA-sequencing analysis, Eva Czirr for adult microglia isolation and culturing advice, Hanxiao Liu and Jeffrey Zhu for technical support, and Swastik P. G. for morphology advice. We thank Sanjana Shroff and Kristin Beaumont for assistance regarding snRNAseq (Single Cell Genomics Core, ISMMS), the Human Immune Monitoring Center (ISMMS) for Olink measurements, and Deanna Benson and Nikos Tzavaras of the Microscopy CoRE and Advanced Bioimaging Center (ISMMS) for advice related to synapse phagocytosis imaging and analysis using Imaris software. Components of some figure panels used BioRender content (https://BioRender.com/7o21lrw). We acknowledge computational and data resources provided by Scientific Computing and Data (ISMMS), supported by the National Center for Advancing Translational Sciences, UL1TR004419, and NIH grants S10OD026880 and S10OD030463. This work was supported by the National Institute on Aging (R01AG061382 (JMC), RF1AG072300 (JMC),1F31AG079604-01A1 (BMH), T32AG049688 (BMH, SMP), and R01AG061382-02S1 (JMC, SMP)).

Author contributions

BMH and JMC conceived and designed experiments, performed data analysis and interpretation, and wrote the manuscript. BMH performed experiments. JMC supervised the research. ACF generated tissue related to neuron-specific TIMP2 deletion, and some tissue for WT and TIMP2 KO mice, with percentage area and activation analysis for select cohorts, aided by AP. SMP dissected hippocampi for sequencing experiments and provided additional expertise to guide sequencing analysis. SFP performed morphology analysis and assisted with tissue isolation for adult microglial cultures. All authors provided input and approved the paper.

747 **Conflict of interests**

748 J.M.C. is listed as a co-inventor on patents for treatment of aging-associated conditions, including
749 use of young plasma administration (US10688130B2) or youth-associated protein TIMP2
750 (US10617744B2), the latter of which was licensed to Alkahest, Inc.

751

752 **References**

753

754 1 Lau, V., Ramer, L. & Tremblay, M.-È. An aging, pathology burden, and glial senescence
755 build-up hypothesis for late onset Alzheimer's disease. *Nature Communications* **14**, 1670
756 (2023).

757 2 Romero-Molina, C., Garretti, F., Andrews, S. J., Marcora, E. & Goate, A. M. Microglial
758 efferocytosis: Diving into the Alzheimer's disease gene pool. *Neuron* **110**, 3513-3533
759 (2022).

760 3 Streit, W. J., Braak, H., Xue, Q.-S. & Bechmann, I. Dystrophic (senescent) rather than
761 activated microglial cells are associated with tau pathology and likely precede
762 neurodegeneration in Alzheimer's disease. *Acta Neuropathologica* **118**, 475-485 (2009).

763 4 Streit, W. J., Sammons, N. W., Kuhns, A. J. & Sparks, D. L. Dystrophic microglia in the
764 aging human brain. *Glia* **45**, 208-212 (2004).

765 5 Hu, Y. *et al.* Replicative senescence dictates the emergence of disease-associated
766 microglia and contributes to Aβ pathology. *Cell Reports* **35**, 109228 (2021).

767 6 Flury, A. *et al.* A neurodegenerative cellular stress response linked to dark microglia and
768 toxic lipid secretion. *Neuron* (2024).

769 7 Brelstaff, J. H. *et al.* Microglia become hypofunctional and release metalloproteases and
770 tau seeds when phagocytosing live neurons with P301S tau aggregates. *Sci Adv* **7**,
771 eabg4980 (2021).

8 Thomas, A. L., Lehn, M. A., Janssen, E. M., Hildeman, D. A. & Chougnet, C. A. Naturally-aged microglia exhibit phagocytic dysfunction accompanied by gene expression changes reflective of underlying neurologic disease. *Scientific Reports* **12**, 19471 (2022).

9 Heneka, M. T. *et al.* NLRP3 is activated in Alzheimer's disease and contributes to pathology in APP/PS1 mice. *Nature* **493**, 674-678 (2013).

10 Zhou, Y. *et al.* Demyelination-derived lysophosphatidylserine promotes microglial dysfunction and neuropathology in a mouse model of Alzheimer's disease. *Cellular & Molecular Immunology* **22**, 134-149 (2025).

11 Hickman, S. E., Allison, E. K. & El Khoury, J. Microglial Dysfunction and Defective β-Amyloid Clearance Pathways in Aging Alzheimer's Disease Mice. *The Journal of Neuroscience* **28**, 8354-8360 (2008).

12 Marschallinger, J. *et al.* Lipid-droplet-accumulating microglia represent a dysfunctional and proinflammatory state in the aging brain. *Nat Neurosci* **23**, 194-208 (2020).

13 Qin, L., Liu, Y., Hong, J. S. & Crews, F. T. NADPH oxidase and aging drive microglial activation, oxidative stress, and dopaminergic neurodegeneration following systemic LPS administration. *Glia* **61**, 855-868 (2013).

14 Castellano, Joseph M. Blood-Based Therapies to Combat Aging. *Gerontology* **65**, 84-89 (2019).

15 Bieri, G., Schroer, A. B. & Villeda, S. A. Blood-to-brain communication in aging and rejuvenation. *Nature Neuroscience* **26**, 379-393 (2023).

16 Castellano, J. M. *et al.* Human umbilical cord plasma proteins revitalize hippocampal function in aged mice. *Nature* **544**, 488-492 (2017).

17 Villeda, S. A. *et al.* Young blood reverses age-related impairments in cognitive function and synaptic plasticity in mice. *Nature Medicine* **20**, 659-663 (2014).

18 Schroer, A. B. *et al.* Platelet factors attenuate inflammation and rescue cognition in ageing. *Nature* **620**, 1071-1079 (2023).

798 19 Katsimpardi, L. *et al.* Vascular and Neurogenic Rejuvenation of the Aging Mouse Brain by
799 Young Systemic Factors. *Science* **344**, 630-634 (2014).
800 20 Yang, A. C. *et al.* Physiological blood–brain transport is impaired with age by a shift in
801 transcytosis. *Nature* **583**, 425-430 (2020).
802 21 Lu, N. *et al. Circulatory proteins shape microglia state and boost phagocytosis* (Cold
803 Spring Harbor Laboratory, 2024).
804 22 Anastasi, F. *et al.* Polygenic proxies of age-related plasma protein levels reveal TIMP2
805 role in cognitive performance. *Res Sq* (2024).
806 23 Britton, R. *et al.* Noncanonical Activity of Tissue Inhibitor of Metalloproteinases 2 (TIMP2)
807 Improves Cognition and Synapse Density in Aging. *eneuro* **10**, ENEURO.0031-0023.
808 (2023).
809 24 Peeney, D. *et al.* Mapping Extracellular Protein–Protein Interactions Using Extracellular
810 Proximity Labeling (ePL). *Journal of Proteome Research* **23**, 4715-4728 (2024).
811 25 Ferreira, A. C. *et al.* Neuronal TIMP2 regulates hippocampus-dependent plasticity and
812 extracellular matrix complexity. *Molecular Psychiatry* **28**, 3943-3954 (2023).
813 26 Nguyen, P. T. *et al.* Microglial Remodeling of the Extracellular Matrix Promotes Synapse
814 Plasticity. *Cell* **182**, 388-403.e315 (2020).
815 27 Cornell, J., Salinas, S., Huang, H.-Y. & Zhou, M. Microglia regulation of synaptic plasticity
816 and learning and memory. *Neural Regeneration Research* **17** (2022).
817 28 Keren-Shaul, H. *et al.* A Unique Microglia Type Associated with Restricting Development
818 of Alzheimer's Disease. *Cell* **169**, 1276-1290.e1217 (2017).
819 29 Almanzar, N. *et al.* A single-cell transcriptomic atlas characterizes ageing tissues in the
820 mouse. *Nature* **583**, 590-595 (2020).
821 30 Yao, Z. *et al.* A high-resolution transcriptomic and spatial atlas of cell types in the whole
822 mouse brain. *Nature* **624**, 317-332 (2023).

823 31 Liberzon, A. *et al.* The Molecular Signatures Database (MSigDB) hallmark gene set
824 collection. *Cell Syst* **1**, 417-425 (2015).
825 32 Shea, J. M. & Villeda, S. A. Microglia aging in the hippocampus advances through
826 intermediate states that drive activation and cognitive decline. *eLife* **13**, RP97671 (2025).
827 33 Oliveros, G. *et al.* Repurposing ibudilast to mitigate Alzheimer's disease by targeting
828 inflammation. *Brain* **146**, 898-911 (2022).
829 34 Avila, J. A. *et al.* PACAP27 mitigates an age-dependent hippocampal vulnerability to
830 PGJ2-induced spatial learning deficits and neuroinflammation in mice. *Brain and behavior*
831 **10**, e01465 (2020).
832 35 Chaudry, O. *et al.* Females exhibit higher GluA2 levels and outperform males in active
833 place avoidance despite increased amyloid plaques in TgF344-Alzheimer's rats. *Scientific*
834 *Reports* **12**, 19129 (2022).
835 36 Corwin, C. *et al.* Prostaglandin D2/J2 signaling pathway in a rat model of
836 neuroinflammation displaying progressive parkinsonian-like pathology: potential novel
837 therapeutic targets. *Journal of Neuroinflammation* **15** (2018).
838 37 Ulrich, J. D. *et al.* In vivo measurement of apolipoprotein E from the brain interstitial fluid
839 using microdialysis. *Molecular Neurodegeneration* **8**, 13 (2013).
840 38 Pait, M. C. *et al.* Novel method for collecting hippocampal interstitial fluid extracellular
841 vesicles (EV(ISF)) reveals sex-dependent changes in microglial EV proteome in response
842 to Abeta pathology. *J Extracell Vesicles* **13**, e12398 (2024).
843 39 Lund, S. *et al.* The dynamics of the LPS triggered inflammatory response of murine
844 microglia under different culture and in vivo conditions. *Journal of Neuroimmunology* **180**,
845 71-87 (2006).
846 40 Cirrito, J. R. *et al.* In Vivo Assessment of Brain Interstitial Fluid with Microdialysis Reveals
847 Plaque-Associated Changes in Amyloid-β Metabolism and Half-Life. *The Journal of*
848 *Neuroscience* **23**, 8844-8853 (2003).

849 41 Castellano, J. M. *et al.* Human apoE isoforms differentially regulate brain amyloid-β
850 peptide clearance. *Sci Transl Med* **3**, 89ra57 (2011).
851 42 Lively, S. & Schlichter, L. C. Microglia responses to pro-inflammatory stimuli (LPS, IFNγ+
852 TNFα) and reprogramming by resolving cytokines (IL-4, IL-10). *Frontiers in cellular*
853 *neuroscience* **12**, 215 (2018).
854 43 Barbera, M. C. *et al.* Increased ectodysplasin-A2-receptor EDA2R is a ubiquitous hallmark
855 of aging and mediates parainflammatory responses. *Nature Communications* **16** (2025).
856 44 Tsuboi, Y. *et al.* Increased hepatocyte growth factor level in cerebrospinal fluid in
857 Alzheimer's disease. *Acta Neurol Scand* **107**, 81-86 (2003).
858 45 Zhao, L. J. *et al.* Associations of the cerebrospinal fluid hepatocyte growth factor with
859 Alzheimer's disease pathology and cognitive function. *BMC Neurol* **21**, 387 (2021).
860 46 Noguchi, C. T., Asavaritikrai, P., Teng, R. & Jia, Y. Role of erythropoietin in the brain.
861 *Critical Reviews in Oncology/Hematology* **64**, 159-171 (2007).
862 47 Esseghir, S. *et al.* A role for glial cell–derived neurotrophic factor–induced expression by
863 inflammatory cytokines and ret/gfrα1 receptor up-regulation in breast cancer. *Cancer*
864 *research* **67**, 11732-11741 (2007).
865 48 Lin, L., Sohar, I., Lackland, H. & Lobel, P. The Human CLN2 Protein/Tripeptidyl-Peptidase
866 I Is a Serine Protease That Autoactivates at Acidic pH. *Journal of Biological Chemistry*
867 **276**, 2249-2255 (2001).
868 49 Smith, P. K., Sen, M. G., Fisher, P. R. & Annesley, S. J. Modelling of Neuronal Ceroid
869 Lipofuscinosis Type 2 in Dictyostelium discoideum Suggests That Cytopathological
870 Outcomes Result from Altered TOR Signalling. *Cells* **8**, 469 (2019).
871 50 Jonas, A. *et al.* Axonally derived matrilin-2 induces proinflammatory responses that
872 exacerbate autoimmune neuroinflammation. *Journal of Clinical Investigation* **124**, 5042-
873 5056 (2014).

874 51 Parkhurst, C. N. *et al.* Microglia promote learning-dependent synapse formation through
875 brain-derived neurotrophic factor. *Cell* **155**, 1596-1609 (2013).
876 52 Czirr, E. *et al.* Microglial complement receptor 3 regulates brain Aβ levels through secreted
877 proteolytic activity. *Journal of Experimental Medicine* **214**, 1081-1092 (2017).
878 53 Safaiyan, S. *et al.* Age-related myelin degradation burdens the clearance function of
879 microglia during aging. *Nature Neuroscience* **19**, 995-998 (2016).
880 54 Machlovi, S. I. *et al.* APOE4 confers transcriptomic and functional alterations to primary
881 mouse microglia. *Neurobiol Dis* **164**, 105615 (2022).
882 55 Tang, J. *et al.* TIMP2 ameliorates blood-brain barrier disruption in traumatic brain injury by
883 inhibiting Src-dependent VE-cadherin internalization. *The Journal of Clinical Investigation*
884 **134** (2024).
885 56 Habib, N. *et al.* Disease-associated astrocytes in Alzheimer's disease and aging. *Nature*
886 *Neuroscience* **23**, 701-706 (2020).
887 57 Ianevski, A., Giri, A. K. & Aittokallio, T. Fully-automated and ultra-fast cell-type
888 identification using specific marker combinations from single-cell transcriptomic data.
889 *Nature Communications* **13**, 1246 (2022).
890 58 Krasemann, S. *et al.* The TREM2-APOE Pathway Drives the Transcriptional Phenotype
891 of Dysfunctional Microglia in Neurodegenerative Diseases. *Immunity* **47**, 566-581.e569
892 (2017).
893 59 Escoubas, C. C. *et al.* Type-I-interferon-responsive microglia shape cortical development
894 and behavior. *Cell* **187**, 1936-1954.e1924 (2024).
895 60 Chen, X. *et al.* A brain cell atlas integrating single-cell transcriptomes across human brain
896 regions. *Nature Medicine* **30**, 2679-2691 (2024).
897 61 Masuda, T. *et al.* IRF8 is a critical transcription factor for transforming microglia into a
898 reactive phenotype. *Cell reports* **1**, 334-340 (2012).

899 62 Przanowski, P. *et al.* The signal transducers Stat1 and Stat3 and their novel target Jmjd3
900 drive the expression of inflammatory genes in microglia. *Journal of Molecular Medicine*
901 **92**, 239-254 (2014).
902 63 Pu, Z. *et al.* Regulation of Microglia-Activation-Mediated Neuroinflammation to Ameliorate
903 Ischemia-Reperfusion Injury via the STAT5-NF-κB Pathway in Ischemic Stroke. *Brain*
904 *Sciences* **12**, 1153 (2022).
905 64 Jayadev, S. *et al.* Transcription factor p53 influences microglial activation phenotype. *Glia*
906 **59**, 1402-1413 (2011).
907 65 Bido, S. *et al.* Microglia-specific *IL-10* gene delivery inhibits neuroinflammation and
908 neurodegeneration in a mouse model of Parkinson's disease. *Science Translational*
909 *Medicine* **16**, eadm8563 (2024).
910 66 Sheikh, A. M. *et al.* Aggregation of Cystatin C Changes Its Inhibitory Functions on
911 Protease Activities and Amyloid β Fibril Formation. *Int J Mol Sci* **22** (2021).
912 67 Ryan, S. K. *et al.* Microglia ferroptosis is regulated by SEC24B and contributes to
913 neurodegeneration. *Nature Neuroscience* **26**, 12-26 (2023).
914 68 Takakura, Y. *et al.* Mitochondrial protein C15ORF48 is a stress-independent inducer of
915 autophagy that regulates oxidative stress and autoimmunity. *Nature Communications* **15**,
916 953 (2024).
917 69 Wang, M. *et al.* Thymosin β4 reverses phenotypic polarization of glial cells and cognitive
918 impairment via negative regulation of NF-κB signaling axis in APP/PS1 mice. *J*
919 *Neuroinflammation* **18**, 146 (2021).
920 70 Subramanian, A. *et al.* Gene set enrichment analysis: A knowledge-based approach for
921 interpreting genome-wide expression profiles. *Proceedings of the National Academy of*
922 *Sciences* **102**, 15545-15550 (2005).
923 71 Jaitin, D. A. *et al.* Lipid-Associated Macrophages Control Metabolic Homeostasis in a
924 Trem2-Dependent Manner. *Cell* **178**, 686-698.e614 (2019).

925 72 Frigerio, C. S. *et al.* The major risk factors for Alzheimer's disease: age, sex, and genes
926 modulate the microglia response to Aβ plaques. *Cell reports* **27**, 1293-1306. e1296 (2019).
927 73 Friedman, B. A. *et al.* Diverse Brain Myeloid Expression Profiles Reveal Distinct Microglial
928 Activation States and Aspects of Alzheimer's Disease Not Evident in Mouse Models. *Cell*
929 *Reports* **22**, 832-847 (2018).
930 74 Heneka, M. T. *et al.* Locus ceruleus controls Alzheimer's disease pathology by modulating
931 microglial functions through norepinephrine. *Proceedings of the National Academy of*
932 *Sciences* **107**, 6058-6063 (2010).
933 75 Izzy, S. *et al.* Nasal anti-CD3 monoclonal antibody ameliorates traumatic brain injury,
934 enhances microglial phagocytosis and reduces neuroinflammation via IL-10-dependent
935 Treg–microglia crosstalk. *Nature Neuroscience* (2025).
936 76 Yousef, H. *et al.* Aged blood impairs hippocampal neural precursor activity and activates
937 microglia via brain endothelial cell VCAM1. *Nature Medicine* **25**, 988-1000 (2019).
938 77 Hemmer, B. M., Philippi, S. M. & Castellano, J. M. Youth-associated platelet-derived
939 chemokine reverses brain aging through neuroimmune mechanisms. *Trends in Molecular*
940 *Medicine* **30**, 10-12 (2024).
941 78 Ayata, P. *et al.* Epigenetic regulation of brain region-specific microglia clearance activity.
942 *Nature neuroscience* **21**, 1049-1060 (2018).
943 79 Hammond, T. R. *et al.* Single-Cell RNA Sequencing of Microglia throughout the Mouse
944 Lifespan and in the Injured Brain Reveals Complex Cell-State Changes. *Immunity* **50**, 253-
945 271.e256 (2019).
946 80 Lee, E.-J. & Kim, H.-S. The anti-inflammatory role of tissue inhibitor of metalloproteinase-
947 2 in lipopolysaccharide-stimulated microglia. *Journal of Neuroinflammation* **11**, 116
948 (2014).
949 81 Sardiello, M. *et al.* A gene network regulating lysosomal biogenesis and function. *Science*
950 **325**, 473-477 (2009).

951 82 Settembre, C. *et al.* TFEB Links Autophagy to Lysosomal Biogenesis. *Science* **332**, 1429-
952 1433 (2011).
953 83 Fadok, V. A. *et al.* Macrophages that have ingested apoptotic cells in vitro inhibit
954 proinflammatory cytokine production through autocrine/paracrine mechanisms involving
955 TGF-beta, PGE2, and PAF. *J Clin Invest* **101**, 890-898 (1998).
956 84 Podleśny-Drabiniok, A., Marcora, E. & Goate, A. M. Microglial Phagocytosis: A Disease-
957 Associated Process Emerging from Alzheimer's Disease Genetics. *Trends in*
958 *Neurosciences* **43**, 965-979 (2020).
959 85 Bohlen, C. J., Bennett, F. C. & Bennett, M. L. Isolation and Culture of Microglia. *Curr*
960 *Protoc Immunol* **125**, e70 (2019).
961 86 Podleśny-Drabiniok, A. *et al.* BHLHE40/41 regulate microglia and peripheral macrophage
962 responses associated with Alzheimer's disease and other disorders of lipid-rich tissues.
963 *Nature Communications* **15**, 2058 (2024).
964 87 Young, M. D. & Behjati, S. SoupX removes ambient RNA contamination from droplet-
965 based single-cell RNA sequencing data. *GigaScience* **9** (2020).
966 88 McGinnis, C. S., Murrow, L. M. & Gartner, Z. J. DoubletFinder: Doublet Detection in Single-
967 Cell RNA Sequencing Data Using Artificial Nearest Neighbors. *Cell Syst* **8**, 329-337.e324
968 (2019).
969 89 Andreatta, M. & Carmona, S. J. STACAS: Sub-Type Anchor Correction for Alignment in
970 Seurat to integrate single-cell RNA-seq data. *Bioinformatics* **37**, 882-884 (2021).
971 90 Miller, S. A. *et al.* LSD1 and Aberrant DNA Methylation Mediate Persistence of
972 Enteroendocrine Progenitors That Support *BRAF*-Mutant Colorectal Cancer. *Cancer*
973 *Research* **81**, 3791-3805 (2021).
974 91 Yu, G., Wang, L. G., Han, Y. & He, Q. Y. clusterProfiler: an R package for comparing
975 biological themes among gene clusters. *Omics* **16**, 284-287 (2012).

976 92 Korotkevich, G., Sukhov, V. & Sergushichev, A. Fast gene set enrichment analysis.
977 *bioRxiv*, 060012 (2019).
978 93 Kang, J. E. *et al.* Amyloid-beta dynamics are regulated by orexin and the sleep-wake cycle.
979 *Science* **326**, 1005-1007 (2009).
980

Figure 1

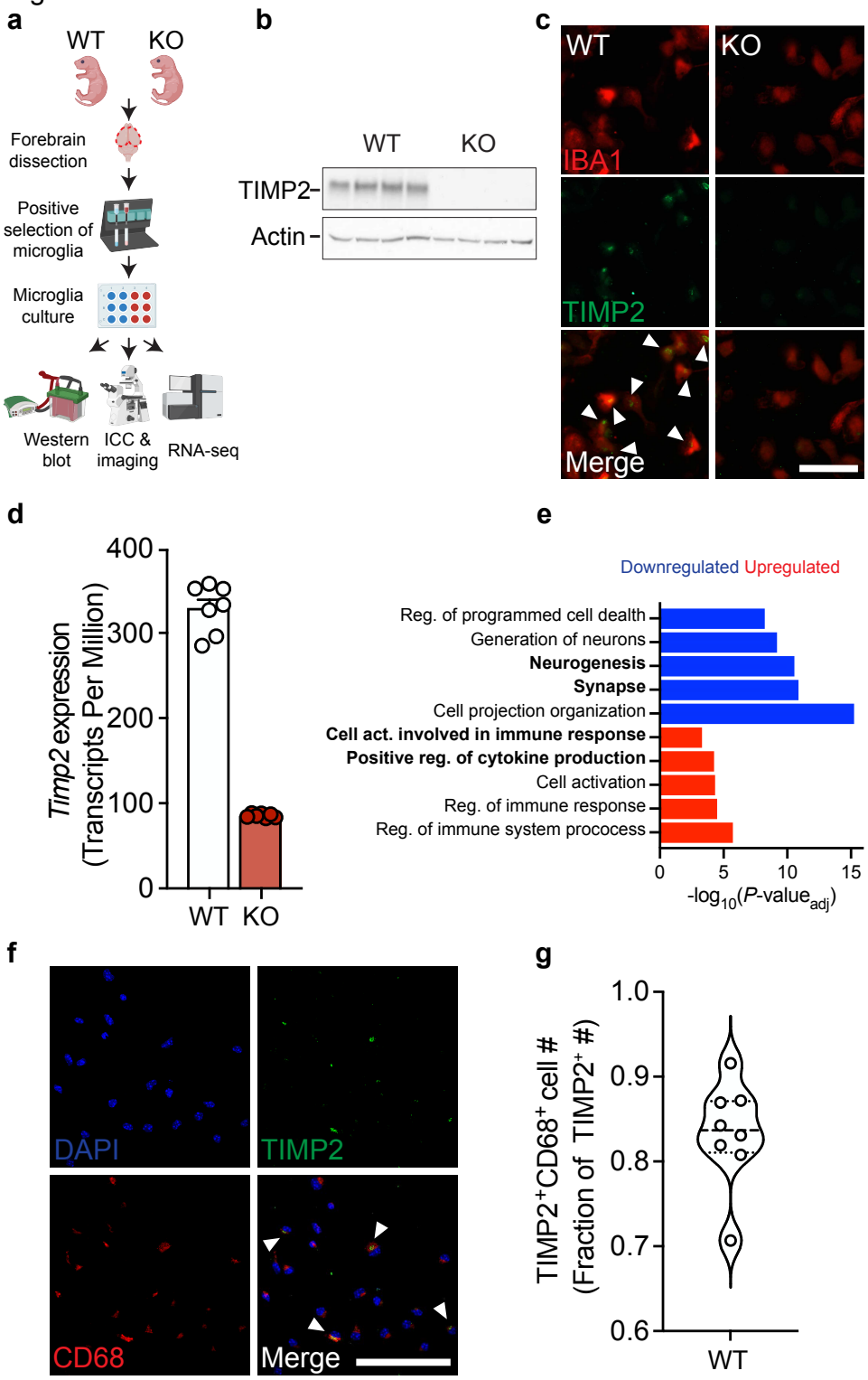
a
WT
KO
Forebrain dissection
Positive selection of microglia
Microglia culture
Western blot
ICC & imaging
RNA-seq
b
WT
KO
TIMP2
Actin
c
WT
KO
IBA1
TIMP2
Merge
d
Timp2 expression (Transcripts Per Million)
400
300
200
100
0
WT
KO
e
Downregulated
Upregulated
Reg. of programmed cell dealth
Generation of neurons
Neurogenesis
Synapse
Cell projection organization
Cell act. involved in immune response
Positive reg. of cytokine production
Cell activation
Reg. of immune response
Reg. of immune system prococess
0
5
10
15
-log10(P-value adj)
f
DAPI
TIMP2
CD68
Merge
g
TIMP2+CD68+ cell # (Fraction of TIMP2+ #)
1.0
0.9
0.8
0.7
0.6
WT

984 **Figure 1. TIMP2 is expressed in microglia and its deletion leads to phenotypes associated**
985 **with increased activation.**
986 **(a)** Schematic diagram of isolation, culturing, and assays performed on TIMP2 KO and WT
987 primary microglia. **(b)** TIMP2 immunoblotting from primary microglia lysates isolated from
988 TIMP2 WT and KO littermates (N = 4 samples per genotype, comprised of 5-6 pups (P5-P8)
989 pooled per sample). **(c)** Representative images from cultures of TIMP2 KO and WT primary
990 microglia (N = 3 pups (P6-P7) pooled per genotype; repeated in 2 additional experiments) stained
991 with anti-TIMP2 and anti-IBA1 antibodies by ICC (scale bar = 100 μm). **(d)** Gene expression
992 (transcript per million) values for *Timp2* from bulk RNAseq experiments from TIMP2 KO and
993 WT primary microglia (N = 7 samples per genotype, with each sample representing a pool of 5
994 pups (P6-P7); sex-matched) with subsequent **(e)** over-representation analysis of GO terms (P_{adj} <
995 0.05) using upregulated and downregulated DEGs in TIMP2 KO vs. WT primary microglia. **(f)**
996 Representative images from WT primary microglia cultures stained by ICC with DAPI, as well as
997 anti-TIMP2 and anti-CD68 antibodies for co-localization analyses (N = 8 mice, 5-6-month-old
998 mice; sex-matched; 2 independent experiments combined; scale bar = 100 μm), with **(g)**
999 quantification of the fraction of $TIMP2^+$ cells that are $TIMP2^+CD68^+$.
1000

Figure 2

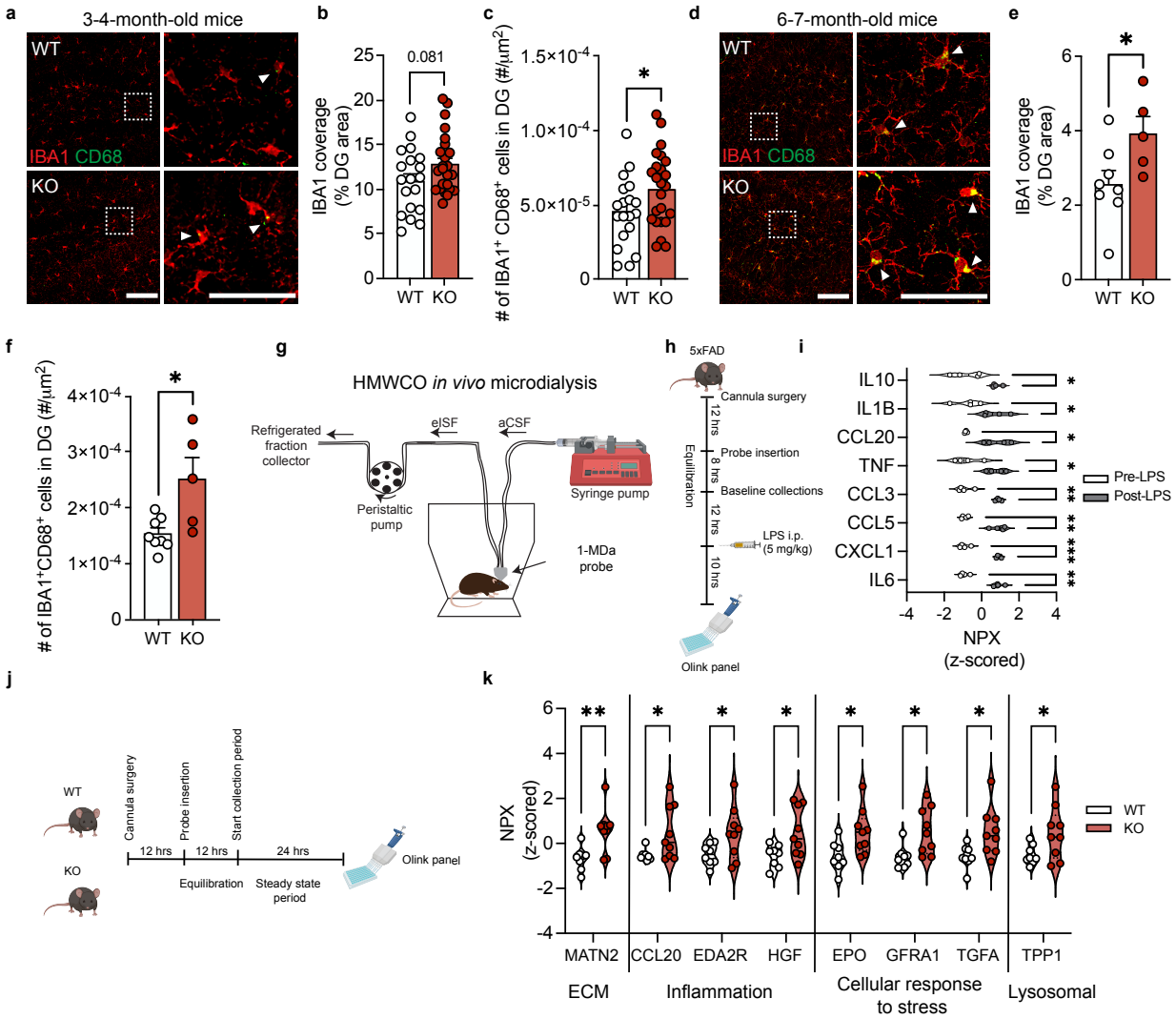

1001

1002 **Figure 2. TIMP2 regulates microglial state and brain extracellular composition *in vivo.***

1003 **(a)** Representative confocal images of dentate gyrus (DG) of 3-4-month-old TIMP2 KO and WT
1004 mice stained with anti-IBA1 and anti-CD68 antibodies (left; scale bar = 100 μm) and magnified
1005 inset (right; scale bar = 50 μm) (N = 9-13 mice per group; sex-matched; arrowheads indicate
1006 $IBA1^{+}CD68^{+}$ cells) with corresponding **(b)** quantification of thresholded DG area covered by
1007 $IBA1^{+}$ staining and **(c)** the number of $IBA1^{+}CD68^{+}$ cells normalized to DG area. **(d)**
1008 Representative confocal images of dentate gyrus (DG) of 6-7-month-old TIMP2 KO and WT mice
1009 stained with anti-IBA1 and anti-CD68 antibodies (left; scale bar = 100 μm) and magnified inset
1010 (right; scale bar = 50 μm) (N = 5-8 mice per group; female mice; arrowheads indicate $IBA1^{+}CD68^{+}$
1011 cells) with corresponding **(e)** quantification of thresholded DG area covered by $IBA1^{+}$ staining and
1012 **(f)** the number of $IBA1^{+}CD68^{+}$ cells normalized to DG area. **(g)** Schematic diagram of the high
1013 molecular-weight cut-off (HMWCO,1-MDa) *in vivo* microdialysis method to dialyze hippocampal
1014 ISF proteins and the corresponding **(h)** timeline of LPS treatment paradigm in mice undergoing
1015 microdialysis (N = 4; 6-7-month-old male 5XFAD mice) with **(i)** brain ISF protein measurements,
1016 represented as z-scored NPX values for significant proteins (paired t-test; $*P < 0.05$, $**P < 0.01$,
1017 $***P < 0.001$). **(j)** Timeline of HMWCO *in vivo* microdialysis experiments to evaluate steady state
1018 levels of hippocampal ISF proteins in 2-3-month-old TIMP2 WT and KO mice (N = 8-9 mice per
1019 group; female mice) with corresponding **(k)** brain ISF protein measurements, represented as z-
1020 scored NPX values for significant proteins (unpaired t-test with Welch's correction; $*P < 0.05$,
1021 $**P < 0.01$). Mean ± SEM. Student's t test used in panels (b-c) and (e-f); $*P < 0.05$.

1022 Figure 3

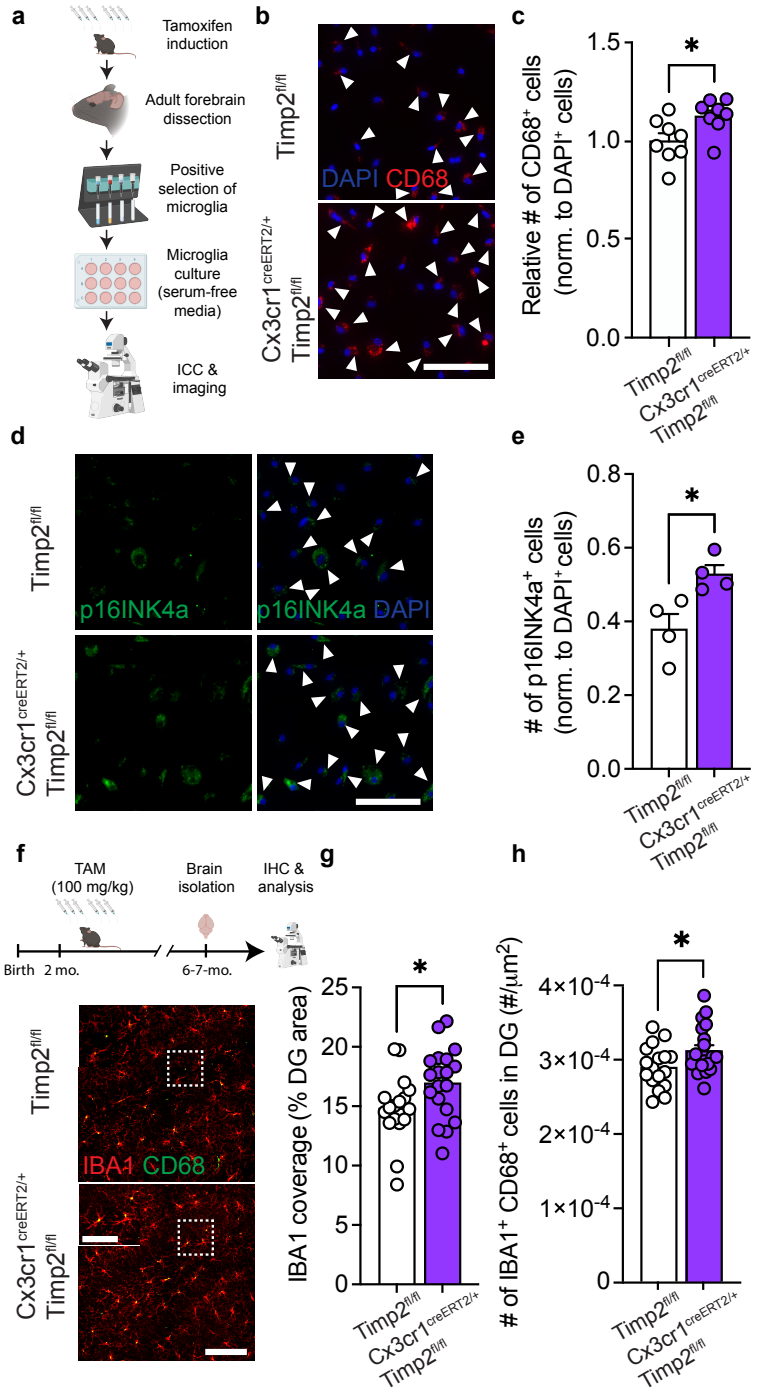

1023 **Figure 3. Removal of microglial TIMP2 increases states of activation and senescence.**

1024 **(a)** Schematic diagram of tamoxifen-inducible microglial deletion of TIMP2 in mice and
1025 subsequent isolation of adult microglia, culturing, and imaging. **(b)** Representative images from
1026 primary microglia cultures of $Timp2^{fl/fl}$ and $Cx3cr1^{CreERT2/+}$;$Timp2^{fl/fl}$ littermates stained by ICC
1027 with DAPI and anti-CD68 antibody (arrowheads indicate $CD68^+$ cells; scale bar = 100 μm) with
1028 corresponding **(c)** quantification of the number of $CD68^+$ cells normalized to total cell number
1029 ($DAPI^+$) (N = 8 mice per group; two independent experiments combined; 5-6-month-old mice;
1030 sex-matched). **(d)** Representative images from primary microglia cultures of $Timp2^{fl/fl}$ and
1031 $Cx3cr1^{CreERT2/+}$;$Timp2^{fl/fl}$ littermates stained by ICC with DAPI and anti-p16INK4a antibody
1032 (arrowheads indicate $p16INK4a^+$ cells; scale bar = 100 μm) with corresponding **(e)** quantification
1033 of the number of $p16INK4a^+$ cells normalized to total number of cells ($DAPI^+$) (N = 4 mice per
1034 group, 7-month-old mice, sex-matched). **(f)** Timeline (top) of Cre induction paradigm with
1035 tamoxifen in $Timp2^{fl/fl}$ control and $Cx3cr1^{CreERT2/+}$;$Timp2^{fl/fl}$ mice and downstream processing of
1036 tissue, with representative confocal images (bottom) of DG of 6-7-month-old $Timp2^{fl/fl}$ and
1037 $Cx3cr1^{CreERT2/+}$;$Timp2^{fl/fl}$ mice stained with anti-IBA1 and anti-CD68 antibodies (scale bar = 100
1038 μm) and magnified inset (scale bar = 50 μm) (N = 17-19 mice per group, sex-matched) with
1039 corresponding **(g)** quantification of DG area covered by anti-IBA1 staining and **(h)** the number of
1040 $IBA1^+CD68^+$ cells normalized to area. Mean ± SEM. *$P < 0.05$; Student's t test.

Figure 4

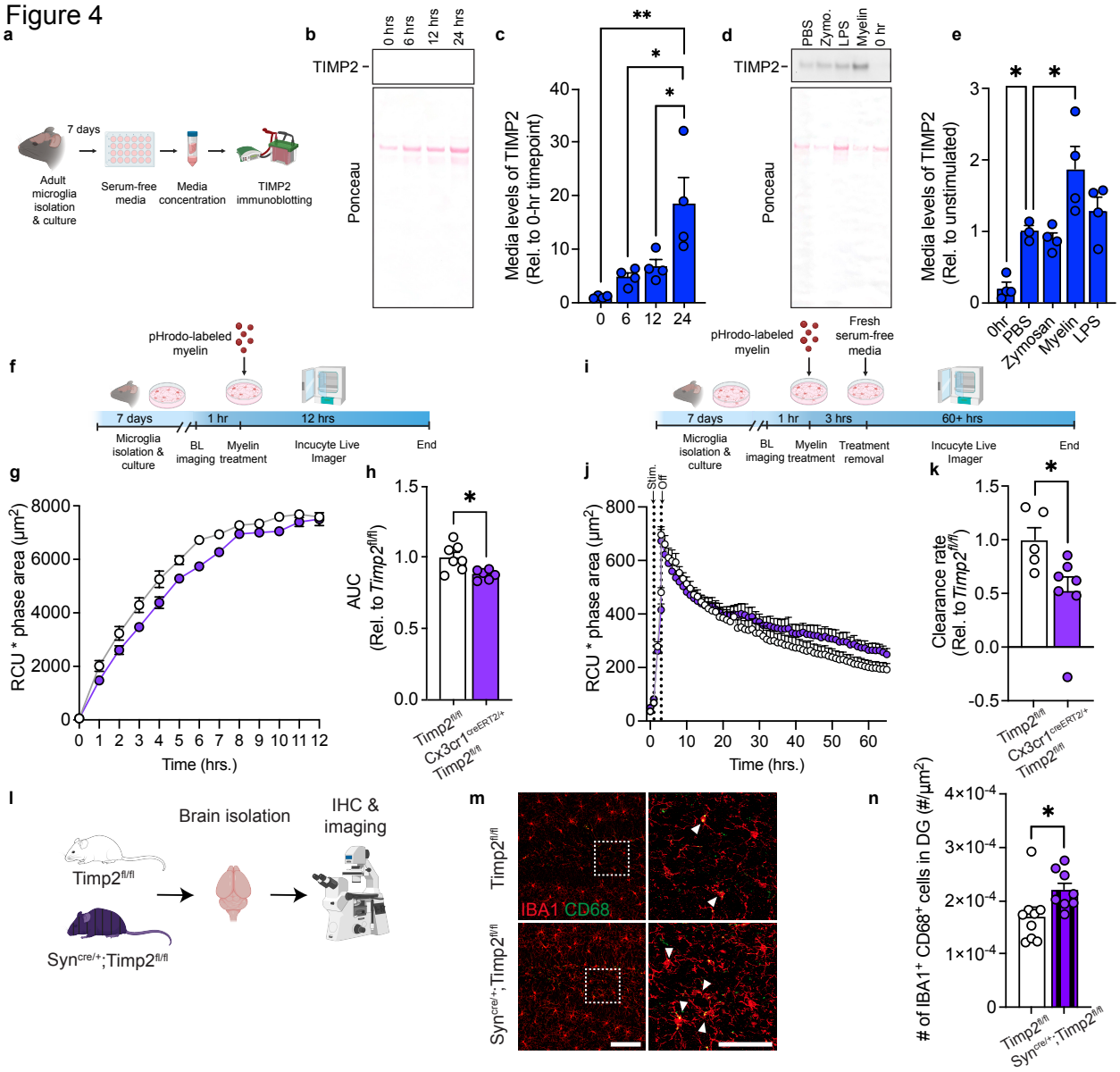

1041

1042 **Fig. 4. TIMP2 is released by microglia and alters microglial response to myelin.**

1043 **(a)** Schematic diagram showing timeline of primary microglia culturing from adult mice and media
1044 assay for TIMP2 immunoblotting experiments. **(b)** TIMP2 immunoblotting (representative) from
1045 conditioned serum-free media from primary microglia isolated from 2-month-old WT mice,
1046 including Ponceau stain (bottom), with corresponding **(c)** TIMP2 band intensity quantification (N
1047 = 4 mice per timepoint; 4 independent experiments combined, with a full timecourse for each
1048 experiment; sex-matched). **(d)** TIMP2 immunoblotting (representative) from conditioned serum-
1049 free media from primary microglia isolated from 2-month-old WT mice at baseline (0 hours with
1050 no treatment) or 12 hours following treatment with either PBS, zymosan (10 μg/mL), myelin (10
1051 μg/mL), or LPS (100 ng/mL), with corresponding **(e)** TIMP2 band intensity quantification (N = 3-
1052 4 mice per treatment; 4 independent experiments combined, with all treatments representing an
1053 experiment; sex-matched). **(f)** Schematic diagram of treatment of adult primary microglia with
1054 pHrodo-labeled myelin and subsequent Incucyte imaging to assess uptake. (**g**) Timecourse from
1055 an experiment with total integrated density (red object mean intensity [RCU, red, *x* average phase
1056 object area (cell, μm^2)) of pHrodo-labeled myelin signal in primary microglia cultured from
1057 tamoxifen-treated 5-7-month-old Cx3cr1$^{CreERT2/+}$;Timp2$^{fl/fl}$ and Timp2$^{fl/fl}$ control mice, with
1058 corresponding **(h)** uptake quantification using area under the curve (AUC; N = 6-7 mice per group;
1059 2 independent experiments combined; sex-matched). **(i)** Schematic of experimental design to
1060 assess clearance of pHrodo-labeled myelin in Cx3cr1$^{CreERT2/+}$;Timp2$^{fl/fl}$ and Timp2$^{fl/fl}$ control mice.
1061 (**j**) Timecourse from an experiment with total integrated density (RCU [red calibrated units]) *x*
1062 average phase object area (cell, μm^2)) of pHrodo-labeled myelin signal in primary microglia
1063 cultured from 5-7-month-old tamoxifen-treated Cx3cr1$^{CreERT2/+}$;Timp2$^{fl/fl}$ and Timp2$^{fl/fl}$ control
1064 mice, with corresponding **(k)** clearance rate quantification (from slopes of regressions),

1065 represented relative to Timp2$^{fl/fl}$ control (N = 5-7 mice per group; 2 independent experiments
1066 combined; sex-matched). **(l)** Schematic diagram of neuron-specific TIMP2 deletion using
1067 *Timp2*$^{fl/fl}$ and Syn$^{Cre/+}$;*Timp2*$^{fl/fl}$ mice for confocal imaging experiments. **(m)** Representative
1068 confocal images of DG from 2-3-month-old Timp2$^{fl/fl}$ and Syn$^{Cre/+}$;Timp2$^{fl/fl}$ littermates stained
1069 with anti-IBA1 and anti-CD68 antibodies (left; scale bar = 100 μm) and magnified inset (right;
1070 scale bar = 50 μm; white arrowheads indicate IBA1^{+}CD68^{+} cells) with corresponding **(n)**
1071 quantification of IBA1^{+}CD68^{+} cell number normalized to DG area (N = 8-9 female mice per
1072 group). Mean ± SEM. *$P < 0.05$, **$P < 0.01$; One-way ANOVA with Tukey's post hoc test (c);
1073 One-way ANOVA with Dunnett's post hoc test (e); Student's t test (h,k,n).

Figure 5

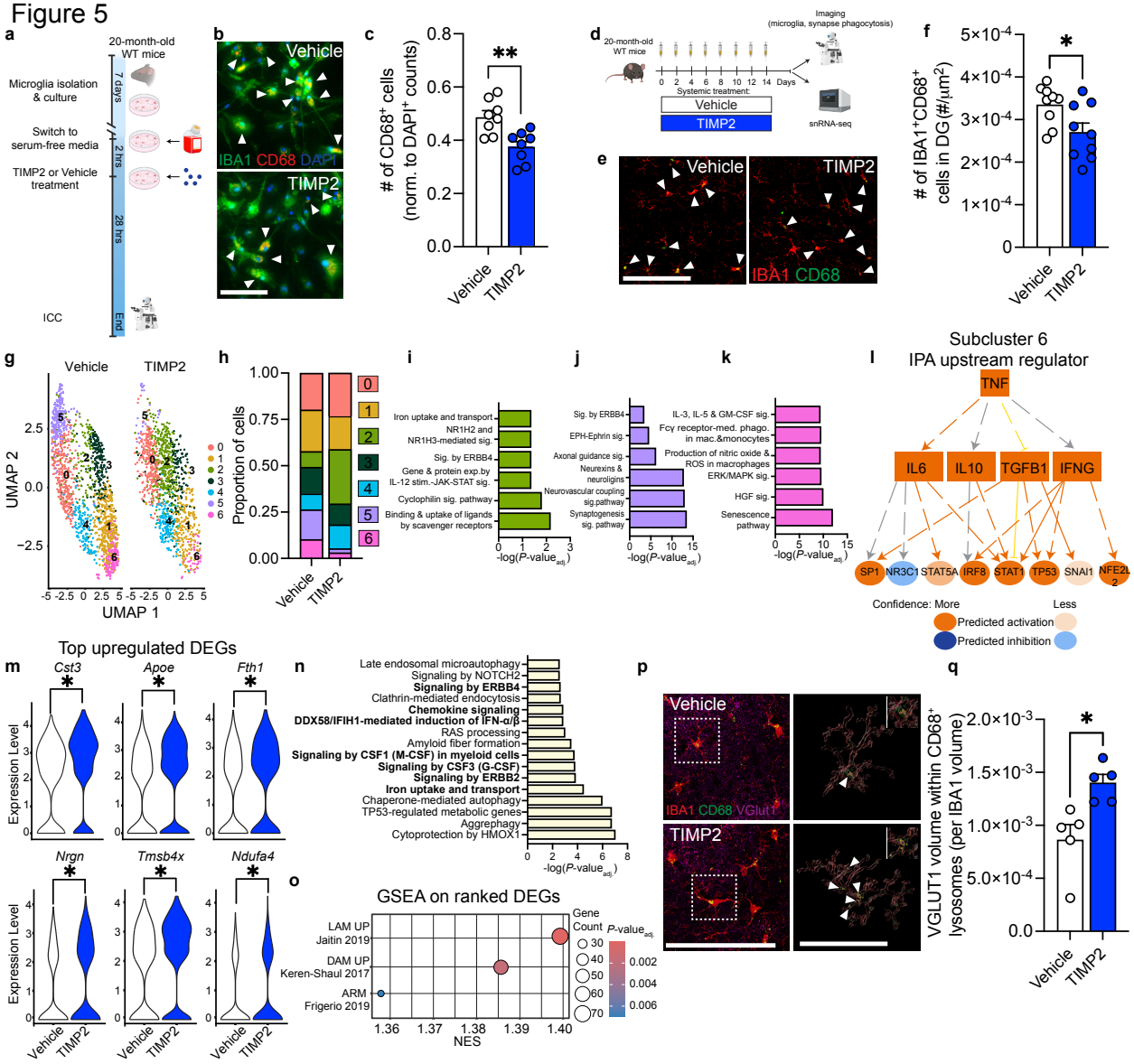

1074

1075 **Fig. 5. Youth-associated TIMP2 alters microglia in aged mice.**

1076 **(a)** Schematic of experimental timeline of microglial isolation from 20-month-old WT mice,
1077 followed by incubation with TIMP2 or vehicle. (**b)** Representative images from cultures of WT
1078 primary microglia stained with anti-IBA1 and anti-CD68 antibodies by ICC (arrowheads indicate
1079 $IBA1^{+}CD68^{+}$ cells; scale bar = 100 μm), with corresponding **(c)** quantification of the number of
1080 $CD68^{+}$ cells normalized to total cell number (N = 8 mice per treatment group, 2 independent
1081 experiments combined; sex-matched). **(d)** Schematic diagram showing paradigm of systemic
1082 treatment with recombinant TIMP2 or vehicle in 20-month-old WT mice, followed by downstream
1083 analyses. **(e)** Representative confocal images of DG from 20-month-old WT mice treated
1084 systemically with TIMP2 or vehicle, stained with anti-IBA1 and anti-CD68 antibodies (scale bar
1085 = 100 μm; white arrowheads indicate $IBA1^{+}CD68^{+}$ cells), with corresponding **(f)** quantification of
1086 number of $IBA1^{+}CD68^{+}$ cells normalized to DG area (N = 9 male mice per group). **(g)** Uniform
1087 Manifold Approximation and Projection (UMAP) plot of hippocampal microglial nuclei (2,831)
1088 isolated from 20-month-old WT mice treated systemically with vehicle or TIMP2 (N = 4 male
1089 mice per group combined as 2 samples per group). **(h)** Proportion of nuclei across microglial
1090 subclusters for each treatment group with corresponding **(i)** Significant canonical pathways from
1091 IPA for marker genes significantly upregulated in subcluster 2, **(j)** subcluster 5, and **(k)** subcluster
1092 6. **(l)** IPA upstream regulator network based on subcluster 6 marker genes, with predicted
1093 relationships for target genes. **(m)** Violin plots of normalized gene expression values from selected
1094 top DEGs; $*P < 0.0001$, from DESeq2 analysis. **(n)** Significant canonical pathways from IPA on
1095 microglial DEGs ($P\text{-value}_{adj.} < 0.05$) from TIMP2-treated vs. vehicle-treated aged mice. **(o)** Dot
1096 plot from Gene Set Enrichment Analysis (GSEA) performed on ranked gene lists derived from
1097 differential expression analysis of microglia following TIMP2 treatment. Significantly enriched

1098 gene sets derived from published transcriptomic states are shown with corresponding Normalized
1099 Enrichment Score (NES), with point size representing number of overlapping genes and color
1100 indicating P-value$_{adj}$. **(p)** Representative confocal images (left) of DG from 20-month-old WT
1101 mice treated systemically with TIMP2 or vehicle, stained with anti-IBA1, anti-CD68, and anti-
1102 Vglut1 antibodies (scale bar = 100 μm), with Imaris-based reconstruction (right) of insetted
1103 microglial volume (red), containing engulfed VGLUT1^{+} puncta (purple with yellow outlines
1104 indicated by white arrowheads) within microglial lysosomes (green) (scale bar = 50 μm). **(q)**
1105 Quantification of the volume of engulfed VGLUT1^{+} signal within CD68^{+} volume, normalized to
1106 microglia volume. Values represent N = 5 mice per group). Mean ± SEM. *$P < 0.05$, **$P < 0.01$;
1107 Student's t test.

1108 Supplementary Figure 1

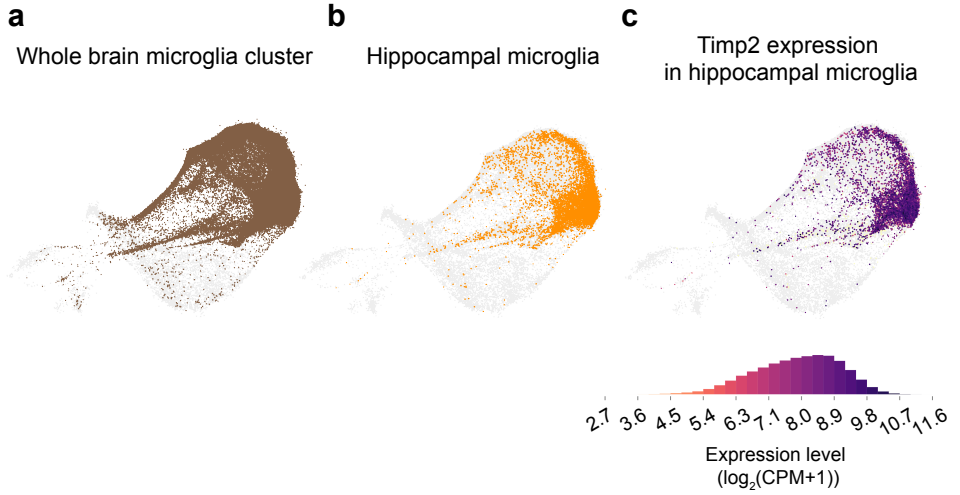

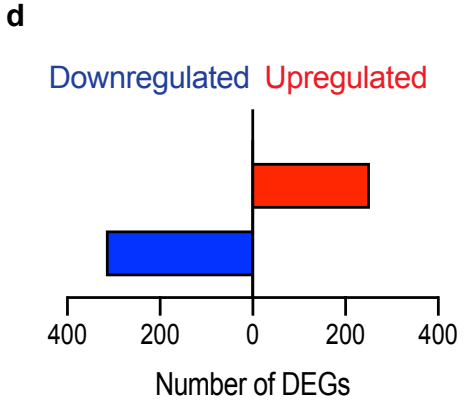

e

Canonical pathways	Predicted activation	*P*-value
Synaptogenesis signaling pathway	Inhibited	1.21E-04
Apoptosis signaling	Inhibited	9.16E-04
Synaptic long-term potentiation	Inhibited	2.49E-03
Rac signaling	Inhibited	4.59E-03
Senescence pathway	Activated	1.89E-03
Interferon gamma signaling	Activated	2.49E-03

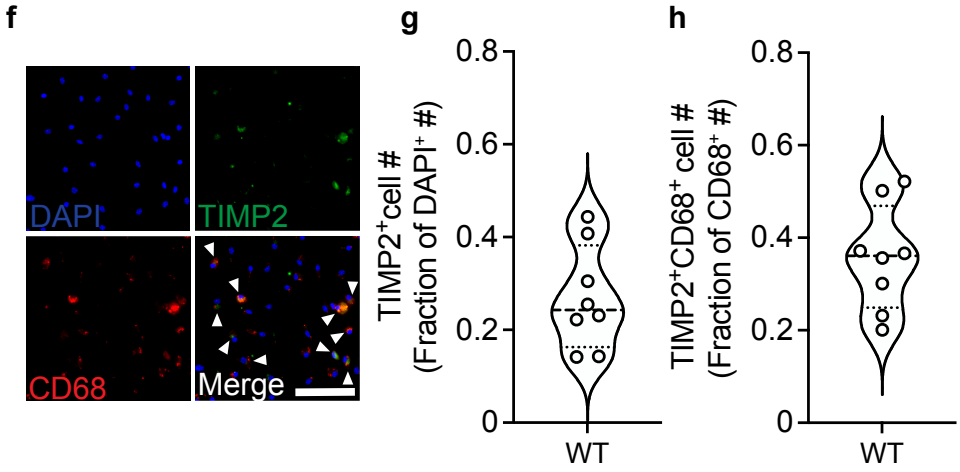

1109 **Supplementary Figure 1. Microglia express TIMP2 protein near lysosomes.**

1110 **(a)** Data from Allen Brain Cell scRNAseq and MERFISH Atlas representing whole brain microglia
1111 (brown), with subsets corresponding to **(b)** hippocampal microglia (orange), and **(c)** TIMP2
1112 expression within hippocampal microglia. **(d)** Number of upregulated and downregulated DEGs
1113 in TIMP2 KO microglia relative to WT microglia (N = 7 samples per genotype, with each sample
1114 representing a pool of 5 pups (P6-P7); sex-matched). **(e)** IPA canonical pathways based on
1115 upregulated and downregulated DEGs in TIMP2 KO and WT microglia from panel (d), with
1116 corresponding predicted inhibition or activation with *P*-values. **(f)** Representative images from
1117 WT primary microglia cultures stained by ICC with DAPI, as well as anti-TIMP2 and anti-CD68
1118 antibodies for overlap analyses (N = 8 mice, 5-6 month-old mice; sex-matched; 2 independent
1119 experiments combined; scale bar = 100 μm), with **(g)** quantification of the number of $TIMP2^+$ cells
1120 as a fraction of $DAPI^+$ cells, or **(h)** the number of $TIMP2^+CD68^+$ cells as a fraction of cells
1121 expressing CD68.

1122 Supplementary Figure 2

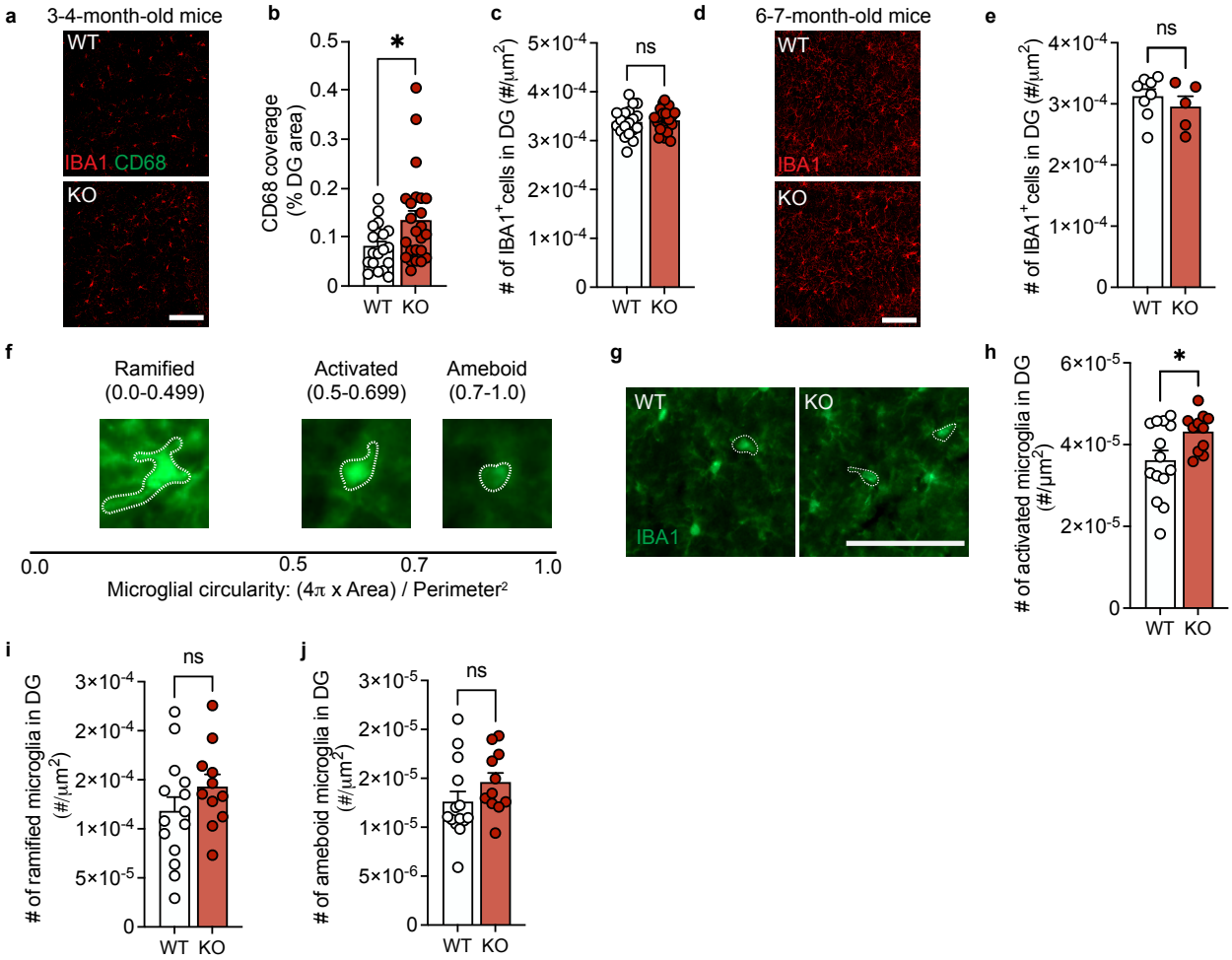

1123 **Supplementary Figure 2. TIMP2 KO mice exhibit altered state and morphology associated**
1124 **with activation.**
1125 **(a)** Representative confocal images of DG from 3-4-month-old WT and TIMP2 KO mice stained
1126 with anti-CD68 and anti-IBA1 antibodies (scale bar = 100 μm) with **(b)** quantification of
1127 thresholded DG area covered by $CD68^+$ staining and **(c)** the number of $IBA1^+$ cells normalized to
1128 DG area (N = 9-13 mice per group; sex-matched). **(d)** Representative confocal images of DG from
1129 6-7-month-old WT and TIMP2 KO mice stained with anti-IBA1 antibody (scale bar = 100 μm)
1130 with **(e)** quantification of the number of $IBA1^+$ cells normalized to DG area (N = 5-8 mice per
1131 group; female). **(f)** Representation of morphology analysis based on microglia circularity, with
1132 representative images for each morphological state according to circularity scale. **(g)**
1133 Representative microscopy images of DG from 6-7-month-old WT and TIMP2 KO mice stained
1134 with anti-IBA1 antibodies, with white dashed lines outlining microglia with "activated"
1135 morphology and corresponding (scale bar = 100 μm) **(h)** quantification of number of microglia
1136 with "activated" microglia (circularity = 0.5-0.699) per DG area. **(i)** Quantification of the number
1137 of microglia with "ramified" morphology (circularity = 0.0-0.499) per DG area, and **(j)** the number
1138 of microglia with "ameboid" microglia (circularity = 0.7-1.0) per DG area. (N = 11-14 mice per
1139 group; sex-matched). Mean ± SEM. $*P < 0.05$; Student's t test; n.s., not significant.

Supplementary Figure 3

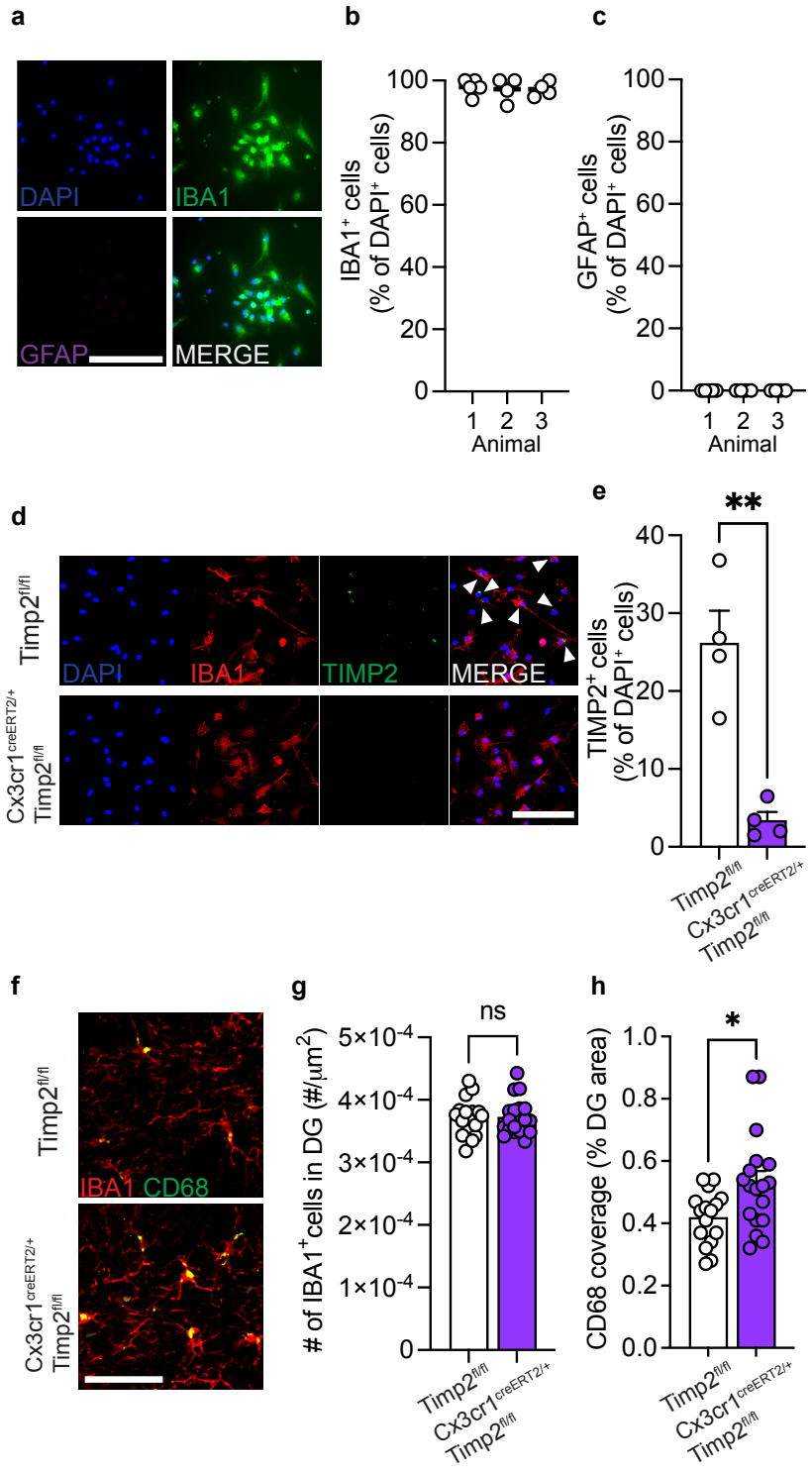

1141 **Supplementary Figure 3. Purity of primary microglia cultures and efficiency of microglia**
1142 ***Timp2* deletion**

1143 **(a)** Representative microscopy images of primary microglia cultures from WT mice stained with
1144 DAPI, anti-IBA1, and anti-GFAP antibodies (scale bar = 100 μm) with **(b)** quantification of $IBA1^+$
1145 cells as a percentage of $DAPI^+$ cells or **(c)** quantification of $GFAP^+$ cells as a percentage of $DAPI^+$
1146 cells (N = 4-5 replicates per mouse from N = 3 mice). **(d)** Representative confocal images from
1147 primary microglia cultures from 5-month-old $Timp2^{fl/fl}$ control and $Cx3cr1^{CreERT2/+}$;$Timp2^{fl/fl}$
1148 littermates stained with DAPI, anti-IBA1 antibody, and anti-TIMP2 antibody (arrowheads indicate
1149 $TIMP2^+$ microglia; N= 4 mice per group; sex-matched; scale bar = 100 μm) with **(e)** quantification
1150 of $TIMP2^+$ cells as a percentage of $DAPI^+$ cell number. **(f)** Representative confocal images of DG
1151 from 6-7-month-old $TIMP2^{fl/fl}$ control and $Cx3cr1^{CreERT2/+}$;$Timp2^{fl/fl}$ littermates stained with anti-
1152 IBA1 and anti-CD68 antibodies (N= 17-19 mice per group; sex-matched; scale bar = 50 μm) with
1153 **(g)** quantification of the number of $IBA1^+$ cells per DG area and **(h)** quantification of DG area
1154 covered by $CD68^+$ staining. Mean ± SEM. *$P < 0.05$; **$P < 0.01$; n.s., not significant. Student's t
1155 test.

Supplementary Figure 4

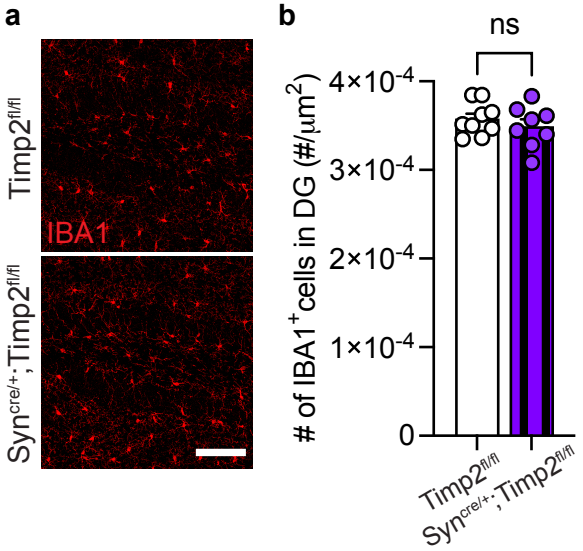

1157 **Supplementary Figure 4. Neuronal deletion of TIMP2 does not alter number of microglia in**

1158 **the dentate gyrus**

1159 **(a)** Representative confocal images of DG from *Timp2*$^{fl/fl}$ and Syn$^{Cre/+}$;*Timp2*$^{fl/fl}$ littermates stained

1160 with anti-IBA1 antibody with corresponding **(b)** quantification of the number of IBA1^{+} cells

1161 normalized to DG area (N = 8-9 mice per group, 2-3-month-old female mice; scale bar = 100 μm).

1162 Mean ± SEM. ; n.s., not significant. Student's t test.

1163 Supplementary Figure 5

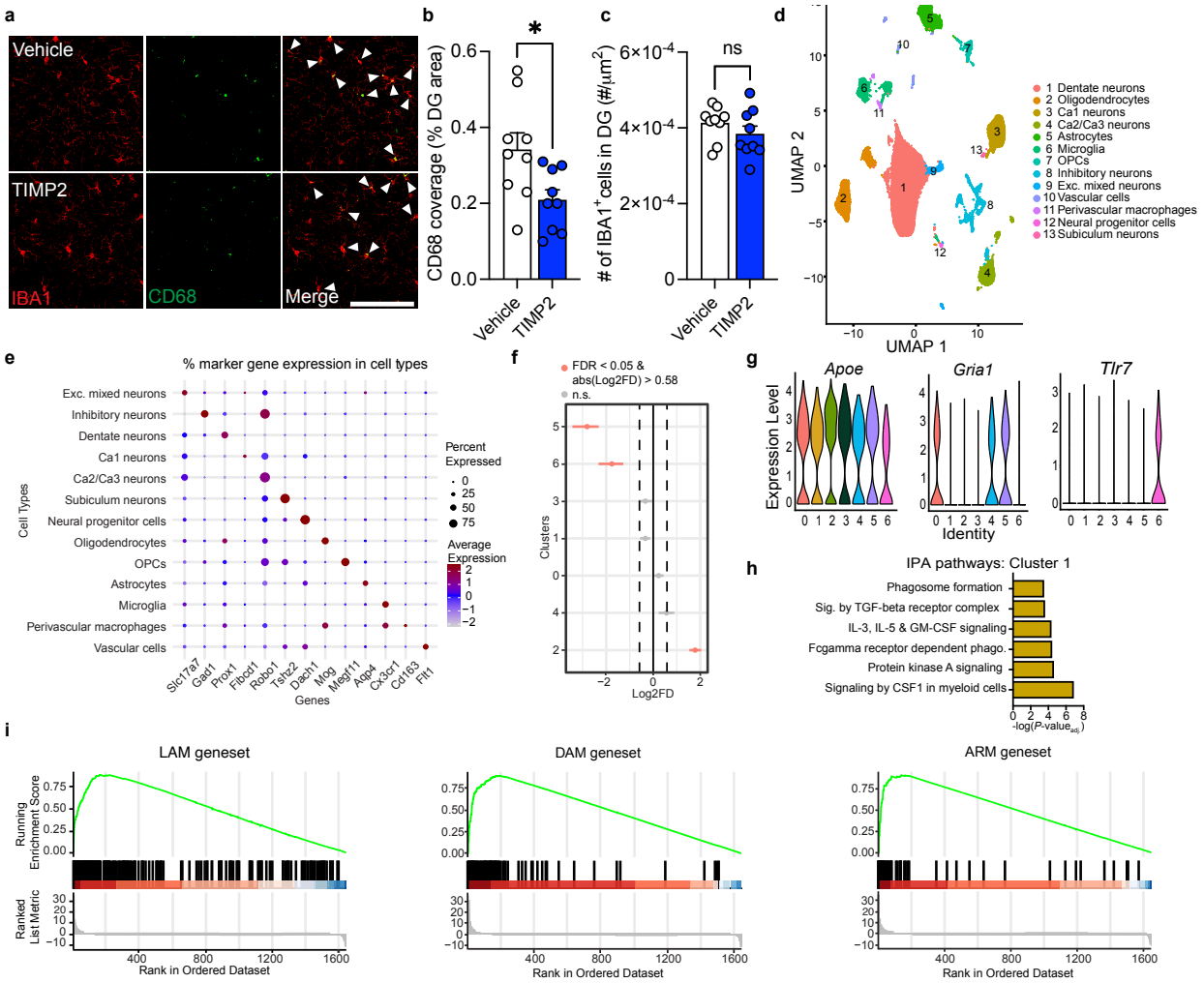

1164 **Supplementary Figure 5. Systemic TIMP2 treatment in aged mice alters microglial state and**
1165 **shifts microglial subclusters.**
1166 **(a)** Representative confocal images of DG from 20-month-old WT mice treated systemically with
1167 TIMP2 or vehicle, stained with anti-IBA1 and anti-CD68 antibodies (scale bar = 100 μm; white
1168 arrowheads indicate $IBA1^{+}CD68^{+}$ cells), with corresponding **(b)** quantification of the percentage
1169 of DG area covered by $CD68^{+}$ staining and **(c)** quantification of the number of $IBA1^{+}$ cells
1170 normalized to DG area (N = 9 male mice per group). **(d)** Uniform Manifold Approximation and
1171 Projection (UMAP) plot of hippocampal nuclei isolated from 20-month-old WT mice treated
1172 systemically with vehicle or TIMP2 (N = 4 male mice per group combined as 2 samples per group).
1173 **(e)** Dot plot of scaled expression of selected marker genes across annotated cell types. Dot size
1174 represents percentage of cells expressing the gene within each cell type, while color indicates the
1175 scaled average expression level of the gene across cells in the respective cluster. **(f)** Differences in
1176 cell proportions for each cluster between treatment conditions. Significant clusters are denoted in
1177 salmon (FDR < 0.05. Log_2 fold-enrichment > 0.58, relative to vehicle-treated mice). **(g)** Violin
1178 plots of selected marker genes across microglial subclusters from Fig. 5h. **(h)** Significant canonical
1179 pathways from IPA for marker genes significantly upregulated in subcluster 1. **(i)** GSEA
1180 enrichment plots for LAM, DAM, and ARM gene sets based on the ranked list of microglial genes
1181 (TIMP2 vs. vehicle). Green lines represent running enrichment score, with vertical black bars
1182 indicating the position of genes from indicated gene sets in the ranked list and gene ranking
1183 direction indicated by color bar (red = upregulated, blue = downregulated).